

Energy and exergy analysis of a cruise ship

Francesco Baldi^a, Fredrik Ahlgren^b, Tuong-Van Nguyen^c, Marcus Thern^d,
Karin Andersson^e

^a*Industrial Process Energy Systems Engineering (IPESE), École Polytechnique Fédérale de Lausanne, 1950, Sion, Switzerland*

^b*Kalmar Maritime Academy, Linnaeus University, Kalmar, Sweden*

^c*Department of Mechanical Engineering, Technical University of Denmark, Lyngby, Denmark*

^d*Energy Sciences, Lund University, Lund SE-22100, Sweden*

^e*Department of Mechanics and Maritime Sciences, Chalmers University of technology, Gothenburg, Sweden*

Abstract

Keywords:

low carbon shipping, energy analysis, exergy analysis, energy efficiency

1. Introduction

1.1. Background

CO₂ emissions from shipping in 2012 amounted to a total of 949 million tonnes, contributing to 2.7% of global anthropogenic CO₂ emissions [1]. Although this contribution appears relatively low, the trend is that shipping will play an even greater role in the future due to the increased transport demand according to all IMO future scenarios [1]. As an example, global transport demand has increased by 3.4% in 2014, compared to a global GBP growth of 2.5% the same year, which shows how shipping tends to rise even faster than global economy [2]. The OECD countries have reduced the CO₂ impact from shipping, but a larger amount has been moved to the non-OECD countries [3]. The fact that shipping needs to even further reduce its CO₂ emissions in the near future is essential for being able to achieve the goals of maintaining the climate below a 2-degree level in 2050 [4].

In addition to considerations related to GHG emissions, an emission control area (ECA) is enforced in the Baltic Sea by the International Maritime Organisation since January 2015. This ECA stipulates that the fuel used

must not contain more than 0.1% sulphur, therefore requiring the use of more expensive distillate fuels. More generally making shipping sustainable is a challenge that will demand growing attention by the shipping industry [3]

In this context, the cruise industry is growing at an even greater pace. Cruise ship passengers have increased from 17.8 million in 2009 to 24.7 million in 2015 [4], and this growth is expected to continue in the coming years [4]. Cruise travels, with an estimated average of 160 kgCO_2 per passenger and per day, are among the most carbon intensive in the whole tourism industry. The contribution of the cruise industry to global CO_2 emissions was estimated to 19.3 Mtons annually in 2010 [5].

The cruise industry has also received much attention for its environmental impact other than in terms of GHG emissions. Cruise ships were shown to have a remarkable negative impact on both air [6] and water [7] quality, and were also pointed as sources of environmental damage from a wider perspective [8]. The fact that cruise ships tend to operate extensively in highly populated and environmental sensitive areas makes the situation all the more worth of attention.

Altogether, these conditions present a challenge to the shipping companies that attempt to reduce their fuel consumption, environmental impact, and operative costs. A wide range of fuel saving solutions for shipping are available and partially implemented in the existing fleet, both from the design and operational perspectives; several specific studies have been conducted on these technologies, and a more detailed treatise would be out of the scope of this work. In this context, it has been acknowledged that the world fleet is heterogeneous, and measures need to be evaluated on a ship-to-ship basis [9]. In this process, a deeper understanding of energy use on board of the specific ship is vital.

1.2. Previous work

The idea of improving the understanding of the behavior of the energy system of a ship is not new. Most of the work published around this subject relates to the use of mathematical models of the ship systems.

Most authors focused on the propulsion part of the problem, as this is often the most relevant energy demand on board. Shi et al. [10] proposed a modeling approach for predicting ship fuel consumption of a cargo/passenger ferry; Theotokoats and Tzelepis [11] applied a similar procedure to the case

of a Handymax product carrier, similarly to Tillig et al. [12], who also added the dynamic element to their predictive model.

The work referenced above allowed improving the understanding of how many operational (such as the ship's speed) and environmental (such as wave height and wind speed) parameters influence the ship's energy performance. These studies, however, are not based on actual measurements of the ship's operations. Also, they focus entirely on the ship's power demand for propulsion. This is a very reasonable practice for most ship types, given that propulsion represent the largest part of the total energy demand, but does not allow improving the knowledge of the remaining part of the system.

Other authors filled the gap by both including electric energy demand, and by basing their work on measurements from actual ship operations. The work presented by Thomas et al. [13] and Basurko et al. [14] shows the application of energy auditing methods to fishing vessels. This approach represents a step forward towards improving the understanding of how energy is used on board during actual ship operations.

More generally, several authors have highlighted the importance of a detailed knowledge of the ship's operational profile in order to appropriately assess and optimize possible alternatives for improving ship energy efficiency [15]. Coraddu et al. [16] started from a statistical analysis of measured ship operations and used the aggregated data, together with a computational model of the vessel, to provide a better prediction of the actual ship's operational efficiency . The importance of considering the operational profile was also showed in the case of the optimization of engine-propeller interaction [17], in the process of retrofitting existing systems [18, 19], and in ship design [20, 21].

Heat demand is rarely a subject of concern on board ships, with some notable exceptions. This is due to a combination of generally low demand and high availability from the waste heat of the engines. In a previous publications by the authors [22], for instance, it is shown that in the case of a product tanker, although the heat demand was estimated to account for roughly 20% of the total energy demand of the ship on a yearly basis, it only contributes to 4.1% of the total fuel consumption (contribution of the auxiliary boilers), while the rest of the demand is fulfilled using waste heat.

It should be noted that, however, much research effort has been devoted, especially in recent times, to the improvement of the efficiency of ship energy systems by recovering the waste heat available from the engines. With reference to different types of technologies, case studies, and designs, the several

authors showed the existance of a quite significant potential for energy saving when WHR systems are employed, ranging from around 1% for single-pressure steam cycles applied to two-stroke engines [23] to more complex systems based on ORCs (up to 10%, [24]) or including the cooling systems as a source of waste heat (over 10%, [25]). The case of the installation of an ORC on board of the vessel investigated in this study (see Section 2.2) was presented in [26], showing a similar potential.

The potential uses for waste heat on board are not limited to improving the efficiency of the power plant. Waste heat is commonly used for fulfilling on board heat demand for spatial heating and freshwater generation [22, 27, 28]; Balaji et al. [29] proposed the use of waste heat for ballast-water systems ; Salmi et al. [30] suggested its use for adsorption refrigeration systems. A detailed review of potential uses for waste heat from marine engines is presented by Shu et al [31].

Some ship types constitute notable examples. On cruise ships the heat demand is significantly higher compared to standard cargo ships. Referring to winter conditions, Marty et al. estimated the instantaneous heat demand of a selected cruise ship to reach roughly 23 MW, compared to an estimated peak of 49 MW for propulsion and electric auxiliaries combined [32].

This shows how the heat from the engines should be considered as a potential resource, rather than a waste, and that there is potential for improvement based on the optimal use of these heat sources. The work presented by the authors in [33] represent a step in this direction; however, there is the need for an increased detail in the estimation of the heat demand.

Exergy analysis provides a more accurate estimation of the potential for energy recovery on board. The application of exergy analysis to the case of ship energy systems is, however, still limited. Dimopoulos et al. [25] showed how the process optimizing the WHR system of a container ship can be more efficient if exergy efficiency, rather than energy efficiency, is used as the target of the optimization; Baldi et al. [22] also analyzed the exergy flows on board of a product tanker, showing that this allows having a more accurate understanding of what parts of the system show potential for improvement ; similar results were obtained by Marty et al. [34], who focused on the power plant of a cruise ship. Koroglu et al. [35] made a step futher also including advanced exergy analysis in their study.

1.3. Aim

Given the existing limitations of the current available information in scientific literature highlighted in the previous section, the objective of this work is the following:

- Analyse the demand of a cruise ship in terms of propulsion power, electric power and heat, based on operational measurements. The lack of existing information with reference to the heat demand is considered a particular element of novelty when compared to existing literature in the subject.
- Analyse the current efficiency of the system, and potential ways to improve it, by means of applying exergy analysis.
- Provide reference operational conditions and typical operational days for further use in the field of energy systems optimization.

2. Method

In this paper, we present the application of energy and exergy analysis (described in Section 2.1) to a cruise ship. This is done for one specific case study vessel, that is described in detail in Section 2.2; in Section Appendix A.1 we present the specifics of the available information, in particular the measured data and the technical documentation; the specific assumptions and methods used for processing the available information into energy and exergy flows are specified in Section 2.4. In these regards, the estimation of the heat demand is treated in a separate section (Section 2.6) as it constitutes a particularly challenging task and is one of the central aspects of this article.

2.1. Energy and exergy analysis

2.1.1. Energy analysis

Energy can be stored, transformed from one form to another (e.g. heat to power) and transferred between systems, but can neither be created nor destroyed (conservation law) [36]. The system under study is the *ship energy system* and is thus taken as control volume. The energy balance can be expressed as:

$$\sum_{\text{in}} \dot{H}_{\text{in}} = \sum_{\text{out}} \dot{H}_{\text{out}} \quad (1)$$

$$\dot{H}_{\text{fuel}} + \dot{H}_{\text{air}} = \sum_{\text{waste}} \dot{H}_{\text{waste}} + \dot{W}_{\text{el}} + \dot{Q}_{\text{heating}} \quad (2)$$

The left-hand side term represents, on a time rate basis, the energy associated with the fuel consumed in the boilers and engines (\dot{H}_{fuel}) and the air used in the combustion processes (\dot{H}_{air}). The right-hand side term denotes the power (\dot{W}_{el}) and heat (\dot{Q}_{heating}) required on-site (e.g. propulsion and fuel heating), and the heat discharged into the environment ($\sum_{\text{waste}} \dot{H}_{\text{waste}}$) with, for instance, the exhaust gases.

The energy flow associated with a material stream is calculated as the sum of the physical and chemical enthalpies, and kinetic and potential energies are neglected. The physical energy is taken as the relative enthalpy, as underlined in [37], and the chemical energy is taken as the lower/higher heating value. The environmental conditions taken for the present analysis are the ambient pressure (1.01 bar) and seawater temperature (measured) .

2.1.2. Exergy analysis

Exergy may be defined as the ‘maximum theoretical useful work (shaft work or electrical work) as the system is brought into complete thermodynamic equilibrium with the thermodynamic environment while the system interacts with it only’ [38]. Unlike energy, exergy is not conserved but some is destroyed because of the irreversible phenomena taking place in real processes (e.g. chemical reactions like combustion). The exergy balance for the system under study can be expressed as:

$$\sum_{\text{in}} \dot{E}_{\text{in}} = \sum_{\text{out}} \dot{E}_{\text{out}} + \dot{E}_d \quad (3)$$

$$\dot{E}_{\text{fuel}} + \dot{E}_{\text{air}} = \sum_{\text{waste}} \dot{E}_{\text{waste}} + \dot{E}_W + \dot{E}_{Q,\text{heating}} + \dot{E}_d \quad (4)$$

The left-hand side term represents, on a time rate basis, the exergy associated with the fuel and air. The right-hand side term denotes the exergy of the waste streams, the exergy transfers with heat and power, and the exergy destroyed in the ship system. Kinetic and potential exergies are neglected,

and the exergy of a given material stream is derived as the sum of the physical and chemical exergies. The chemical exergy is calculated based on the reference environment of [39], and its value is approximatively equal to the higher heating value for hydrocarbon fuels. The exergy destruction can be calculated from the Gouy-Stodola theorem [37].

The exergy balance may alternatively be formulated as:

$$\dot{E}_p = \dot{E}_f - \dot{E}_d - \dot{E}_l \quad (5)$$

where \dot{E}_p is called the exergy product, and corresponds to the desired output of the system, in exergy terms (for example, the power produced in an engine). \dot{E}_f denotes the exergy fuel, and represents the resources spent to drive the studied process (for instance, the fuel used in a combustion process). The last term \dot{E}_l corresponds to the losses of a system, such as the heat discharged into the environment with cooling water.

2.1.3. System performance

The following indicators are used to evaluate the system performance:

- the exergy efficiency ε , defined as the ratio between the exergy product and fuel of a given component or system

$$\varepsilon = \frac{\dot{E}_p}{\dot{E}_f} \quad (6)$$

- the efficiency defect λ , presented in the work of Kotas [37], defined as the fraction of the total exergy input destroyed in the successive irreversible processes

$$\lambda = \frac{\dot{E}_d}{\dot{E}_{in,tot}} \quad (7)$$

- the irreversibility share δ_i , suggested in the work of Tsatsaronis [40], defined as the ratio between the exergy destroyed in the i -th component in relation to the exergy destroyed in the entire system

$$\delta_i = \frac{\dot{E}_{d,i}}{\dot{E}_{d,tot}} \quad (8)$$

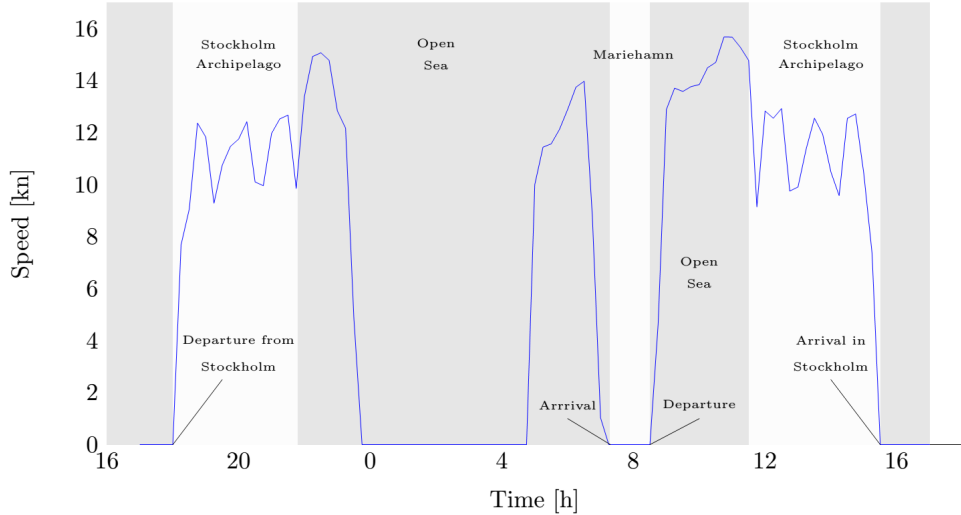


Figure 1: Reference operational profile (ship speed vs time) for the case study

2.2. Case study vessel

The energy and exergy analysis are here applied to a specific cruise ship operating daily cruises in the Baltic Sea between Stockholm and the island of Åland. The ship is 176.9 m long and has a beam of 28.6 m, and has a design speed of 21 knots. The ship was built in Aker Finnyards, Raumo Finland in 2004.

The ship has a capacity of 1800 passengers and has several restaurants, night clubs and bars, as well as saunas and pools. This means that the energy system regarding the heat and electricity demand is more complex than a regular cargo vessel in the same size. Typical ship operations, although they can vary slightly between different days, are represented in Figure 1. It should be noted that the ship stops and drifts in open sea during night hours before mooring at its destination in the morning, if allowed by weather conditions.

The ship systems are summarized in Figure 2. The propulsion system is composed of two equal propulsion lines, each made of two engines, a gearbox, and a propeller. The main engines are four Wärtsilä 4-stroke Diesel engines (ME) rated 5850 kW each. All engines are equipped with selective catalytic reactors (SCR) for NO_x emissions abatement. Propulsion power is needed whenever the ship is sailing; however, it should be noted that the ship rarely sails at full speed, and most of the time it only needs one or two engines operated simultaneously.

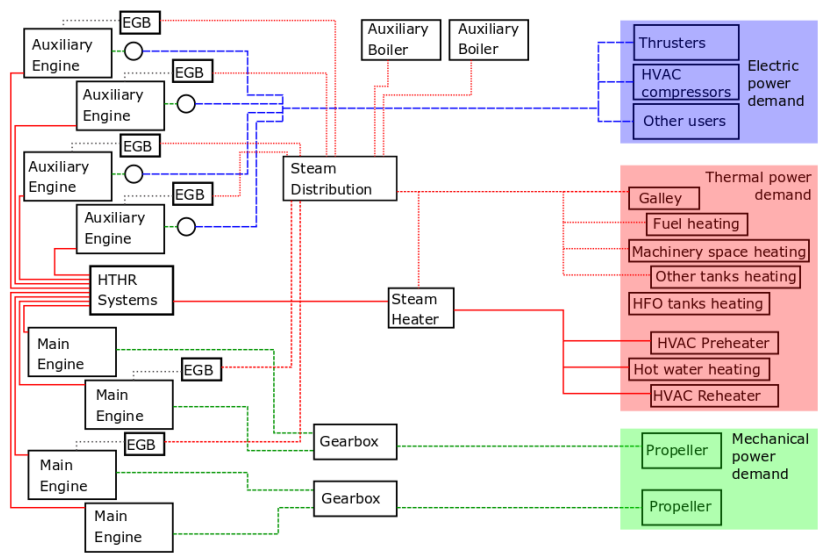


Figure 2: Layout of the case study energy systems

Auxiliary power is provided by four auxiliary engines (AE) rated 2760 kW each. Auxiliary power is needed on board for a number of alternative functions, from pumps in the engine room to lights, restaurants, ventilation and entertainment for the passengers.

Auxiliary heat needs are fulfilled by the exhaust gas steam generators (HRSG) located on all four AEs and on two of the four MEs or by oil-fired auxiliary boilers (mainly when in port, or during winter), by the heat recovery on the HT cooling water systems (HRHT), and by the auxiliary, oil fired boilers (AB). The heat is needed for passenger and crew accommodation, as well as for the heating of the highly viscous heavy fuel oil used for engines and boilers. This last part, however, is drastically reduced since the 1st of January 2015, as new regulations entering into force require the use of low-sulphur fuels, which require a much more limited heating.

2.3. Data gathering and pre-processing

The operational data was collected on board from the ships' machine logging and surveillance system. The data sampling rate was selected to 15 minutes, automatically calculated as averages over the respective periods by the on board data logging systems, as an acceptable compromise between accuracy and computational time required for the data processing. Data consistency was checked individually by creating a descriptive statistic and a histogram of each measurement. A filter was applied by setting up a pre-defined maximum and minimum value.

Since measurements of ambient and seawater temperature from onboard logging systems were not available for the whole dataset, we used measurements taken from SMHI database for Landsort lighthouse for the seawater, and the lighthouse Svenska Högarna for the ambient temperature, both located along the route of the vessel.

2.4. Ship energy system modeling

Not all of the variables required to perform a full energy and exergy analysis of the system are available from measurements. In some cases, they are measurable, but not measured (e.g. some temperatures, mass flows, etc.). In other cases, they are simply impossible, or impractical, to measure (e.g. specific enthalpy, specific entropy). For this reason, part of the ship systems needed to be modeled in order to derive the unknown variables.

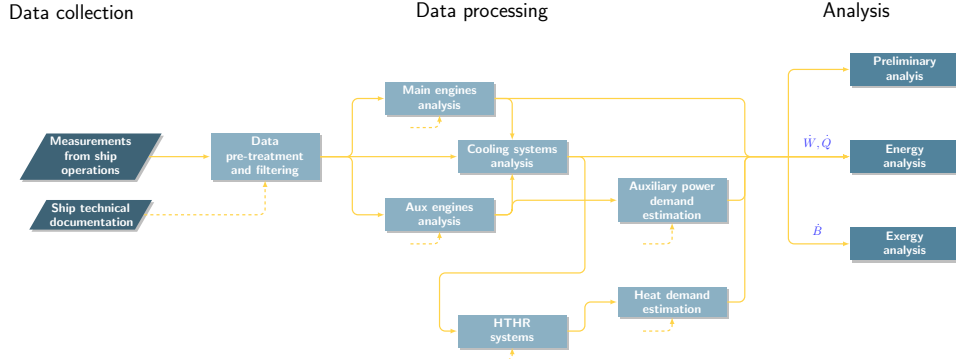


Figure 3: Overview of the data processing from inputs to outputs

The main principles applied to the modeling are presented in the following sections and summarized in Figure ??, while a more thorough description and validation of the different approaches is presented in the Appendix.

2.4.1. Diesel engines

The Diesel engines are the only power source of the system, subdivided in four main engines uniquely devoted to propulsion and four auxiliary engines used for on board electric power generation. The energy and exergy analysis of the engines is not limited to the boundary of the system, but is brought to the detail of the different components that constitute the engine systems, as shown in Figure 4.

In the case of the main engines, the engine power output was not measured and needed to be estimated. In this work, we calculated the engine power output based on measurements of engine fuel rack position (used as a proxy of the mass of fuel injected per cycle) and of the engine speed (see equations 9 to 11). In the case of the auxiliary engines, instead, direct measurements of the power generated by each engine were available.

$$\dot{m}_{fuel} = \dot{m}_{fuel,des} \left(a_0 + a_1 \frac{frp}{frp_{des}} \right) \frac{\omega}{\omega_{des}} \quad (9)$$

$$\eta_{ME} = a_0 + a_1 \frac{\dot{m}_{fuel}}{\dot{m}_{fuel,des}} + a_2 \left(\frac{\dot{m}_{fuel}}{\dot{m}_{fuel,des}} \right)^2 \quad (10)$$

$$\dot{W}_{ME} = \dot{m}_{fuel} \eta_{ME} LHV \quad (11)$$

For both auxiliary and main engines, part of the relevant internal variables are not measured (particularly with relation to the bypass valves) and this

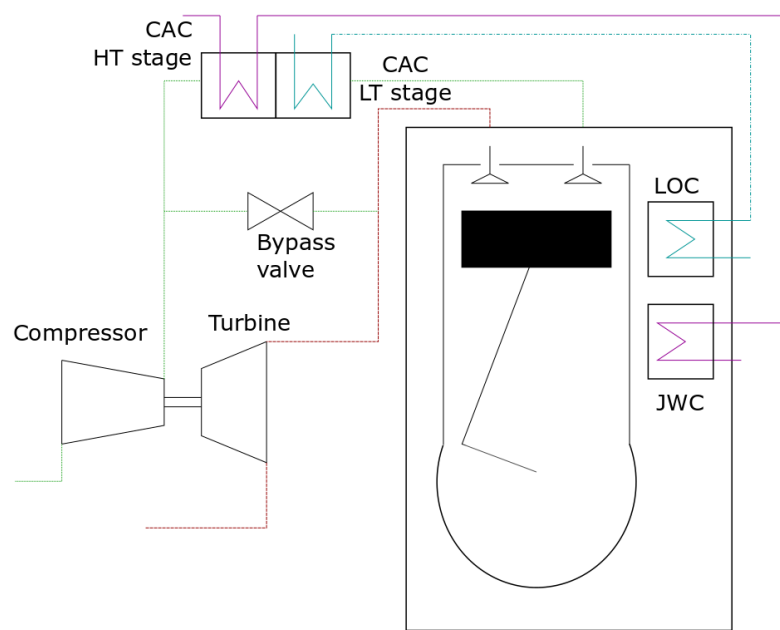


Figure 4: Schematic representation of the Diesel engines and their connections to the cooling systems

required to determine them based on modeling the heat and mass balance of the engine. Values for temperatures, mass flows and energy flows for different engine loads are provided in the Appendix A.2, for both main and auxiliary engines.

2.5. Electric power demand

The total electric power demand of the system is easily estimated as the sum of the power generated by the four auxiliary engines, that is directly measured on the electrical side of the generators and has a rather high accuracy.

$$P_{el,tot} = \sum_1^4 P_{AE_i} \quad (12)$$

The ship is equipped with a number of different systems, including lighting, navigational systems, pumps and compressors, etc. However, none of the individual contributions is directly measured, hence estimations of the energy demand of individual consumers need to be based on indirect measurements. In this paper only the contributions of the HVAC and the bow thrusters are identified separately from the remaining parts of the system. More details about the methods employed in this process are provided in Appendix REF.

2.6. Heating and cooling systems

The case study ship is not provided with any means to directly measure the heat demand (e.g. steam flow meters), and it was hence necessary to provide estimations based on other measurements and assumptions. The heat demand is subdivided among the contributions of the HVAC preheater and re heater ($\dot{Q}_{HVAC,PH}$ and $\dot{Q}_{HVAC,RH}$), the hot water heater (\dot{Q}_{HWH}), the HFO heaters (\dot{Q}_{HH}) the tank heating systems for HFO and other liquids (\dot{Q}_{HTH} and \dot{Q}_{TH}), the machinery space heating (\dot{Q}_{MSH}) and other tanks (\dot{Q}_{OT}). The heat generation is instead composed of the contribution of the exhaust gas boilers ($\dot{Q}_{EGB,ME,i}$ and $\dot{Q}_{EGB,AE,i}$), the heat recovery from the high temperature cooling systems ($\dot{Q}_{HTHR,j,i}$) and the boilers (\dot{Q}_{AB}). The

heat demand and generation are summarized in equations 13 and 14.

$$\dot{Q}_{gen} = \sum_{i=2,3} \dot{Q}_{EGB,ME,i} + \sum_{i=1:4} \dot{Q}_{EGB,AE,i} + \sum_{j=ME,AE,i=1:4} \dot{Q}_{HTHR,j,i} + \dot{Q}_{AB} \quad (13)$$

$$\dot{Q}_{dem} = \dot{Q}_{HVAC,PH} + \dot{Q}_{HVAC,RH} + \dot{Q}_{HWH} + \dot{Q}_{HH} + \dot{Q}_{TH} + \dot{Q}_G + \dot{Q}_{OT} + \dot{Q}_{HTH} + \dot{Q}_{MSH} \quad (14)$$

(15)

The ship's cooling systems are designed similarly to most ships and divided in two cooling systems operated at two separate temperature levels: the high temperature (HT) cooling systems (70-90°C) and the low temperature (LT) cooling systems (40-60°C). The cooling systems provide the necessary cooling to the engines, to the steam systems and to all other components on board. An overview of the ship heating and cooling systems is provided in Figure ??.

All values not directly measured in the cooling systems were calculated based on mass and energy balances. Mass flows were determined based on measurements of the pressure in the system and on the performance curves of the cooling pumps as provided in the engine project guides. The main view of the ship heating and cooling systems is presented in Figure 5.

ADD TABLE WITH LEGEND

The determination of the heat demand is the most challenging in the analysis of ship energy systems, as extensive and appropriate measurements related to this contribution are rarely available. In this case the limited data available was fit with assumptions related to the behavior of the energy system and to the daily repartition of the heating demand. A more detailed description of this procedure is provided in Appendix REF.

2.7. Operational mode

The ship operates in different conditions, and it can be useful to provide a separate analysis depending on the operational mode. The four operational modes identified for the selected case study, together with the conditions applied to the dataset to uniquely identify each time step to a separate operational mode, are given as follows:

High speed sailing Ship speed above 15 kn

Low speed sailing Ship speed between 4 and 15 kn

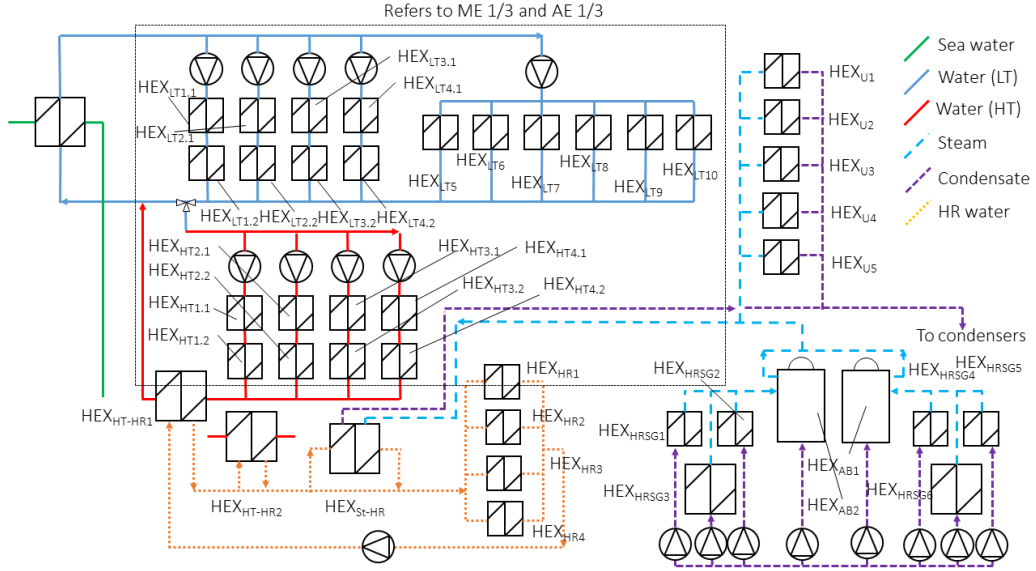


Figure 5: General view of the ship heating and cooling systems

Maneuvering Ship speed between 2 and 4 knots OR Thrusters power larger than 0

Port stays / ship drifting All other points

2.8. Determination of typical operational conditions

Improving the performance of a ship requires a detailed analysis of the energy demands to optimize the dimensioning and operation of the technologies and processes to install on-board. It requires the analysis of the hourly, daily and seasonal variations of the heat/power consumption, operating (e.g. ship speed) and external conditions (e.g. air temperature). However, gathering and processing those data may be time-consuming because of the high number of points to assess. It is therefore desirable to reduce this large quantity of information while keeping the relevant details on the relations between the variables of interest. One way is to represent these yearly profiles in a limited number of representative (typical) periods, avoiding the repetition of similar data sets. Clustering consists of grouping such sets in a single group (cluster) so that the items in the same group are more like each other than to those belonging to other groups. Several algorithms are introduced in the literature to partition these datasets. The one selected in this work

is the Lloyds (k-means) algorithm [41], which is a non-deterministic method computationally faster than conventional hierarchical tools. The approach applied by Fazlollahi et al. [42] was used to select the optimum number of clusters (N_k). It (N_k) should be as low as possible for data handling purposes, while preserving a high accuracy of the retrieved data. It builds on the calculation of three criteria:

1. the average intra-cluster distance to assess the density of each cluster, preferably small;
2. the average inter-cluster distance to assess the distance between each, preferably high;
3. the expected square error, which is a statistical measure suggested by Pham et al..

In parallel, the cluster quality was systematically evaluated by calculating the following performance indicators:

1. the profile deviation (deviation between original and typical period profiles), $\sigma_{profile}$;
2. the deviation from the load duration curve of the average values of each period, σ_{CDC} ;
3. the relative error in load duration curve deviation $ELDC$;
4. the maximum duration load curve difference Δ_{MLDC} ;
5. the number of periods with relative errors Δ_{prod} higher than 7%.

This set of performance objectives is defined as a set of constraints with an upper limit that should be respected when minimizing the number of clusters, applying the e-constraints algorithm. The dataset is further reduced by partitioning each typical day into a set of segments using a similar approach. The aim of the present clustering is to identify typical periods that are appropriate for improving the thermodynamic performance of ship energy systems. It can be achieved through either reducing the external energy demands (better energy management), e.g. with storage systems or internal recovery, or through implementing new technologies that result in higher fuel-to-demand efficiencies (better energy conversion). Hence, the attributes that are the primary focus of this study are:

1. the total power consumption, including the mechanical and electrical loads;

2. the total heating demand, further divided into the low- and high-temperature needs, which is related to the external temperature;
3. the total exergy destruction on-board, which quantifies the thermodynamic performance of the ship energy systems.

A one-year data with 35,040 time steps (sampling of 15 minutes) was selected and divided into typical periods based on these three attributes. The clustering approach proposed by Fazlollahi et al. [42] provides as output typical days having the same data frequency as the original time series (in this case, 15 minutes). From a computational perspective, however, this might not necessarily be the most efficient sampling. Operating conditions within a certain cluster (typical day) are often nearly constant for a longer time, suggesting that a variable time resolution would lead to a lower dimensionality of the data while retaining most of the original information. To this purpose, in this paper we employ the Adaptive Piecewise Constant Approximation (APCA) approach proposed by Keogh et al. [43]

3. Results and discussion

3.1. Exploratory analysis

In this section, we observe and analyze direct measurements from ship systems, with no pre-processing, that are expected to have an influence on the energy analysis.

Figures 6a and 6b represent the time evolution and the distribution over the year of the ambient air and sea water temperature. The relatively low temperatures that are experienced by the case study ship during its operations rise expectations for a high space heating demand and to a relatively low for summer HVAC electric power demand. On the other hand, the fact that, in summer, air temperatures reach up to 26 degrees Celsius justify the existence of an HVAC unit that can also operate in cooling mode.

Figure 7 represents the distribution of the ship speed. The ship operates for almost the entire year according to a fixed schedule, while there are a couple of periods (particularly during the summer months) when the ship operates at higher speed. In Figure 8 it can be also observed that the ship spends a relatively large amount of time in port. These remarks suggest that, in spite of the high installed power of the main engines, the energy demand for propulsion is expected to be relatively low.

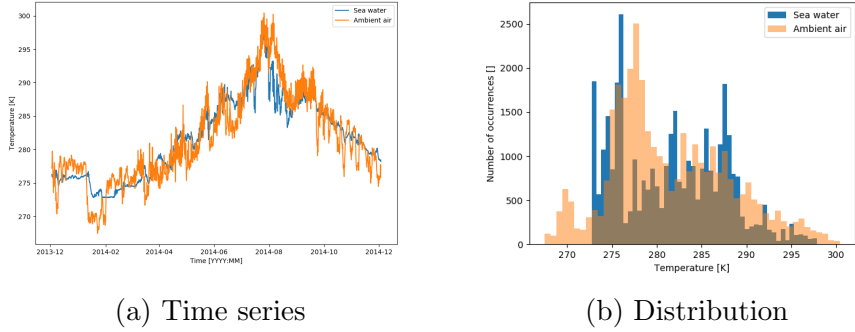


Figure 6: Statistical representation of measured air and sea water temperatures based on yearly data. Landsort, 2014

Figures 9 and 10 show the frequency of the load at which each of the engines (main and auxiliary engines, respectively) is operated. In the case of the main engines, it can be observed that they are operated mostly at loads between 30% and 60%, despite the optimal load for the engines being located around 85%. This is a consequence of both the low speed at which the ship is generally operated, and of the fact that the two shaft lines are operated independently, and hence do not allow the use of only one of the four engines at high load.

In the case of the auxiliary engines, a larger difference between how the engines are operated can be observed. AE-3 is generally more often operated, as it is the engine that is run in port with clean fuels. On the other hand, it seems that AE-4 is operated rarely, which might be due to maintenance issues during the selected period of analysis.

3.2. Energy analysis

The ship energy demand is first subdivided among the different types of consumers. The evolution of the demands of propulsion, electric power, and heat over time during a typical voyage is shown in Figures 11 and 12, representing a winter and a summer day respectively. As expected, the heating demand in winter is higher than in summer [2800-4500 kW vs 1100-2900 kW], as a consequence of the reduced need for compartment heating. On the other hand, the electric power demand behaves inversely, ranging around 1900 kW during the reference winter day (peaks are connected to the use of thrusters in port for maneuvering) and around 2300 kW during the reference summer day, where the difference is mostly associated to the demand of the HVAC

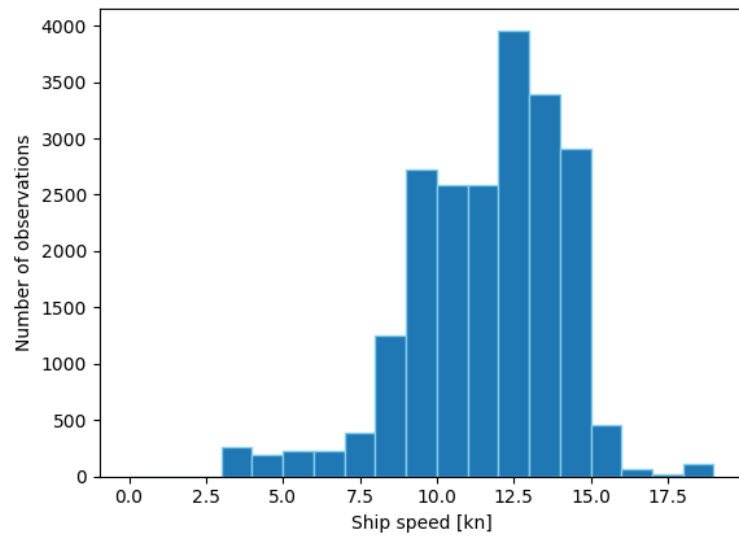


Figure 7: Yearly distribution of ship speed

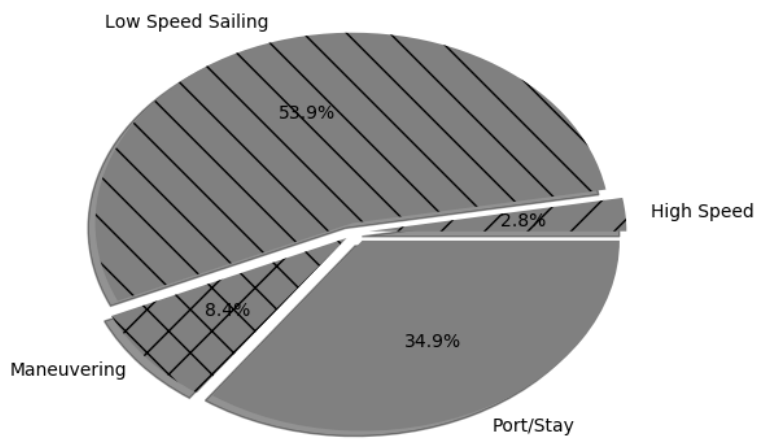


Figure 8: Operational time by mode

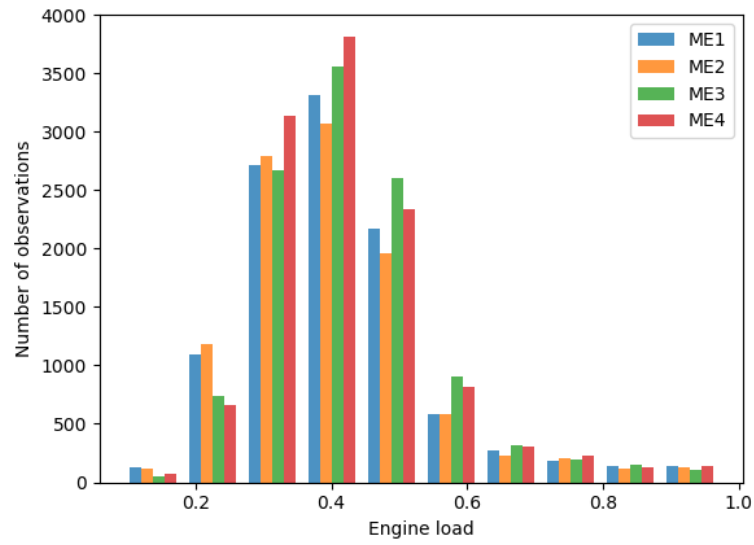


Figure 9: Yearly load distribution, main engines

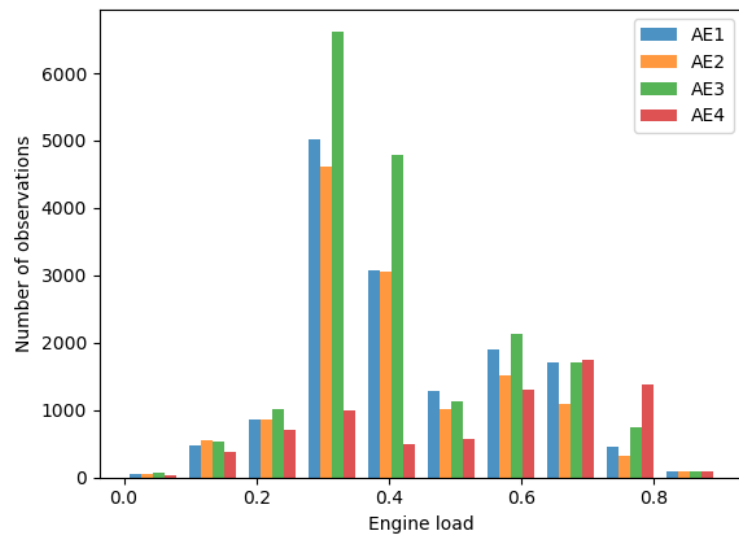


Figure 10: Yearly load distribution, auxiliary engines

compressors. Looking at the yearly cumulated demand, nearly 50% of the total energy demand is related to ship propulsion (see Figure 13), while the remaining portion is approximately equally split between electric energy and heat demand.

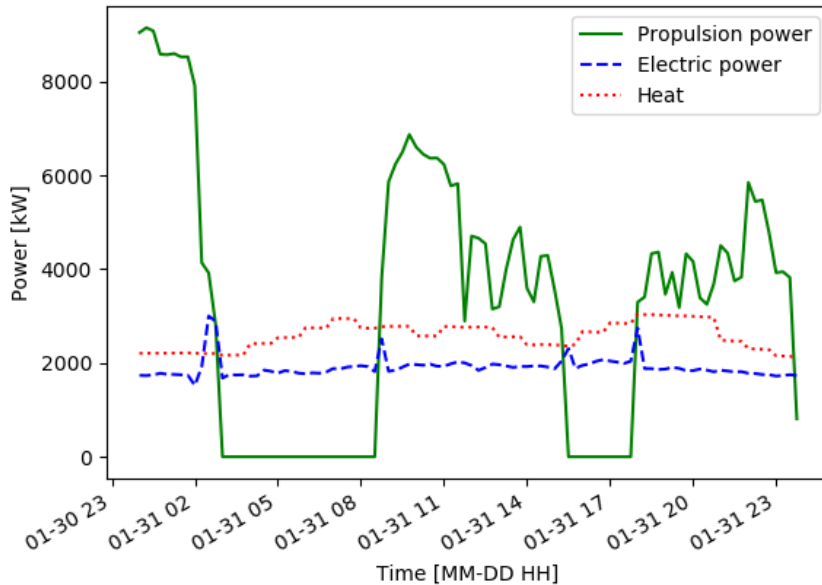


Figure 11: Energy demand during a day of operations, Winter (31 Jan)

Within the electric energy demand, the HVAC systems only represent a minor contribution (3%), as it is only present for a few months during summer. This is not surprising, since it can be observed that (see Figure 6b) the air is always below 27°C, and rarely above 17°C. Also the thrusters, although their instantaneous power demand is high, are only used for a very short time each day and, hence, their total contribution to the ship electrical energy demand is limited to 1.5%.

Heat recovery has a large impact on the overall external heat demand (see Fig. 15). The exhaust gas boilers and the heat recovery on the HT-water fulfill almost 75% of the yearly demand for heating, leaving only the remaining 25% to be provided by oil-fired auxiliary boilers. The contribution of the HRSG and the HTHR is substantially constant throughout the year

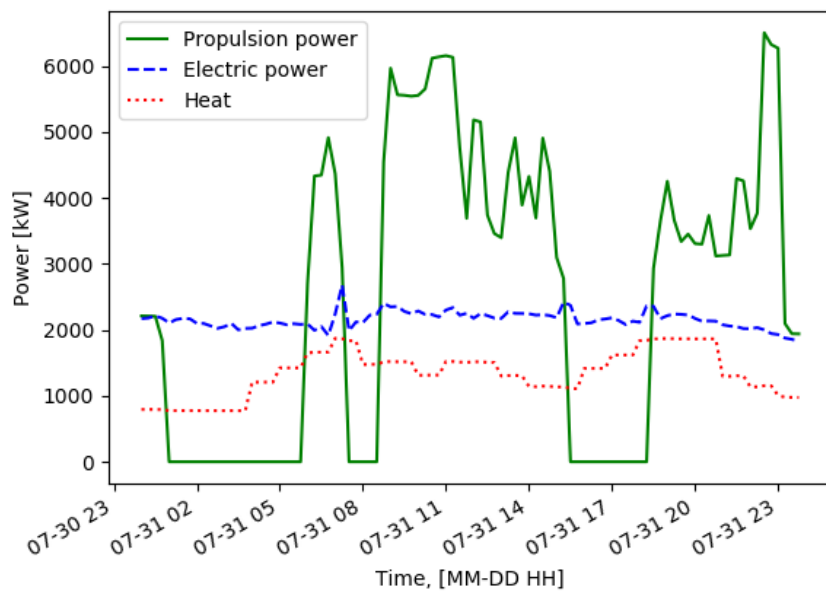


Figure 12: Energy demand during a day of operations, Summer (31 Jul)

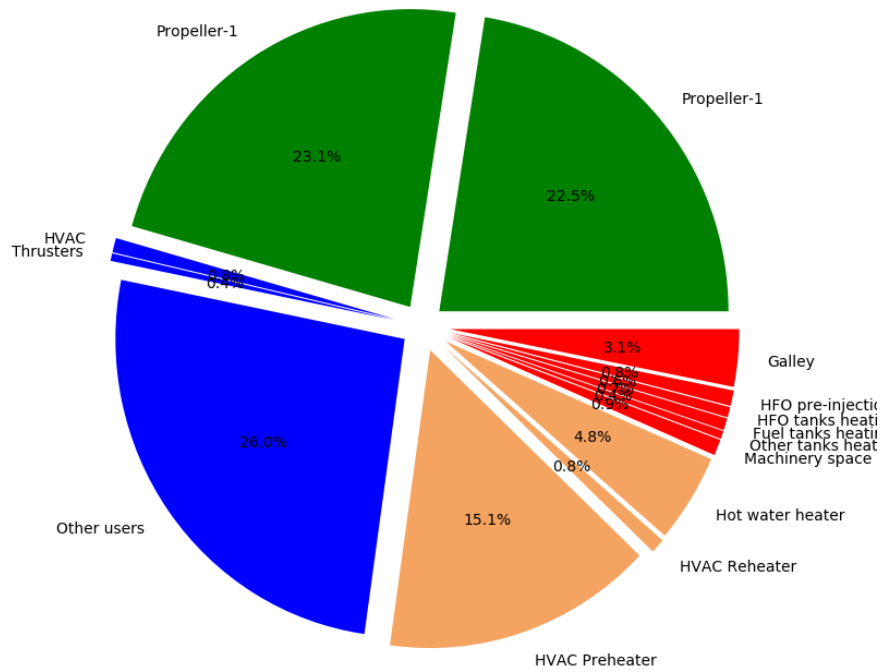


Figure 13: Energy demand, aggregated data for one year of operations

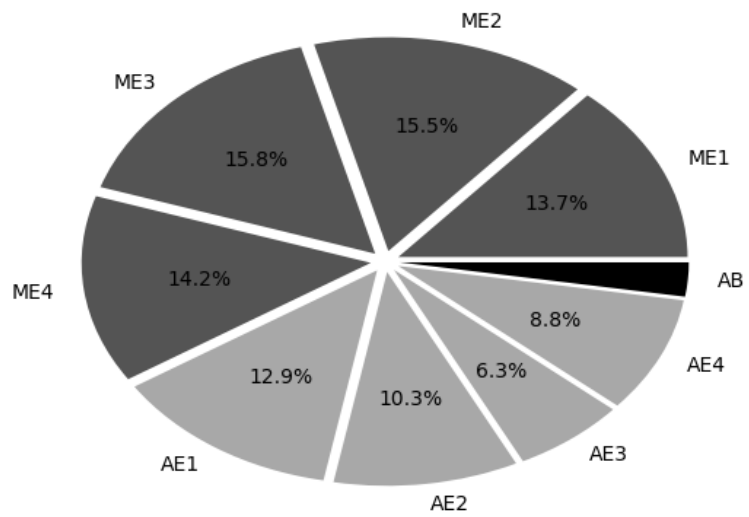


Figure 14: Energy generation, aggregated data for one year of operations

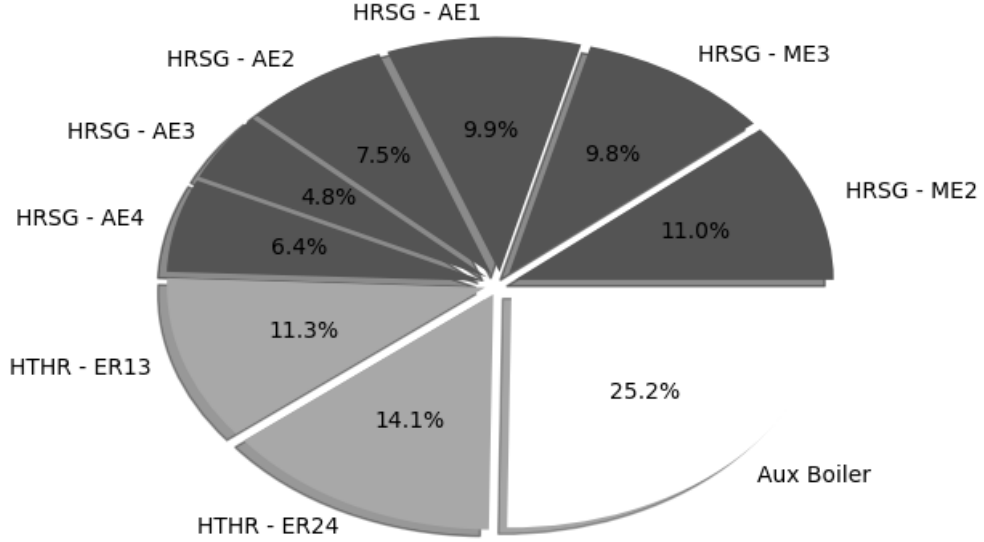


Figure 15: Share of thermal power generated from on board heat systems

(Fig. 16), while the auxiliary boilers are used to cover the peaks and the winter increased baseload.

On the heating demand side, the HVAC pre-heater represents the largest contributor (56%) to the annual heating demand, followed by the hot water heater (18%) and by the galley (11%). In multi-season central HVAC systems the pre-heater is generally used for the main heating contribution during winter, while the re-heater is only used for peak demand, or for adjusting the delivery air temperature during summer, thus explaining the large contribution of the former. The relatively large share of the hot water heater can instead be related to the fact that these systems are used during all seasons.

The full Sankey diagram representation of the energy flows on board is provided in Figure 17.

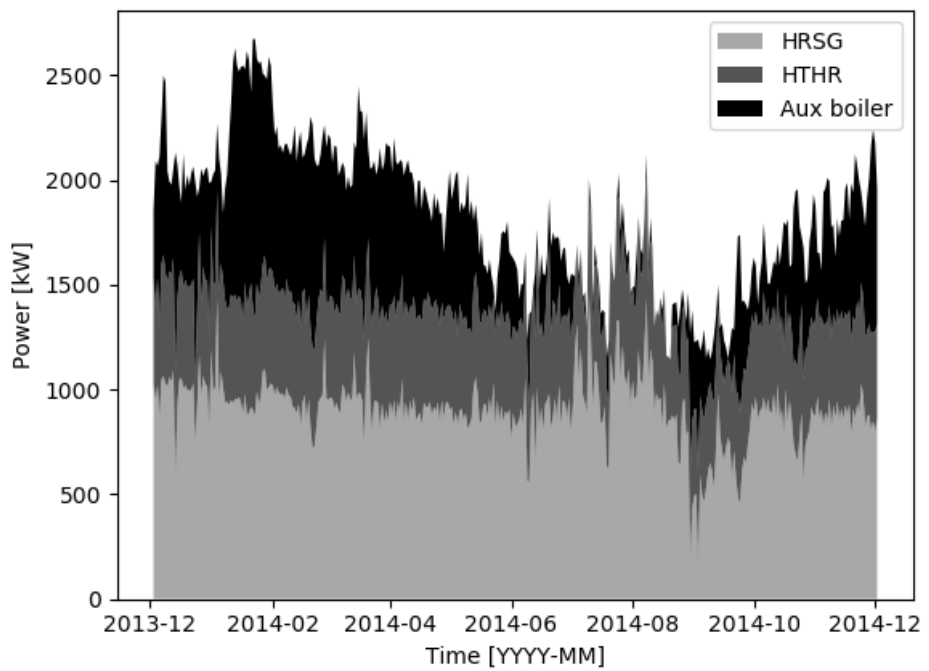


Figure 16: Time series representation of the thermal power generated from on board heat systems

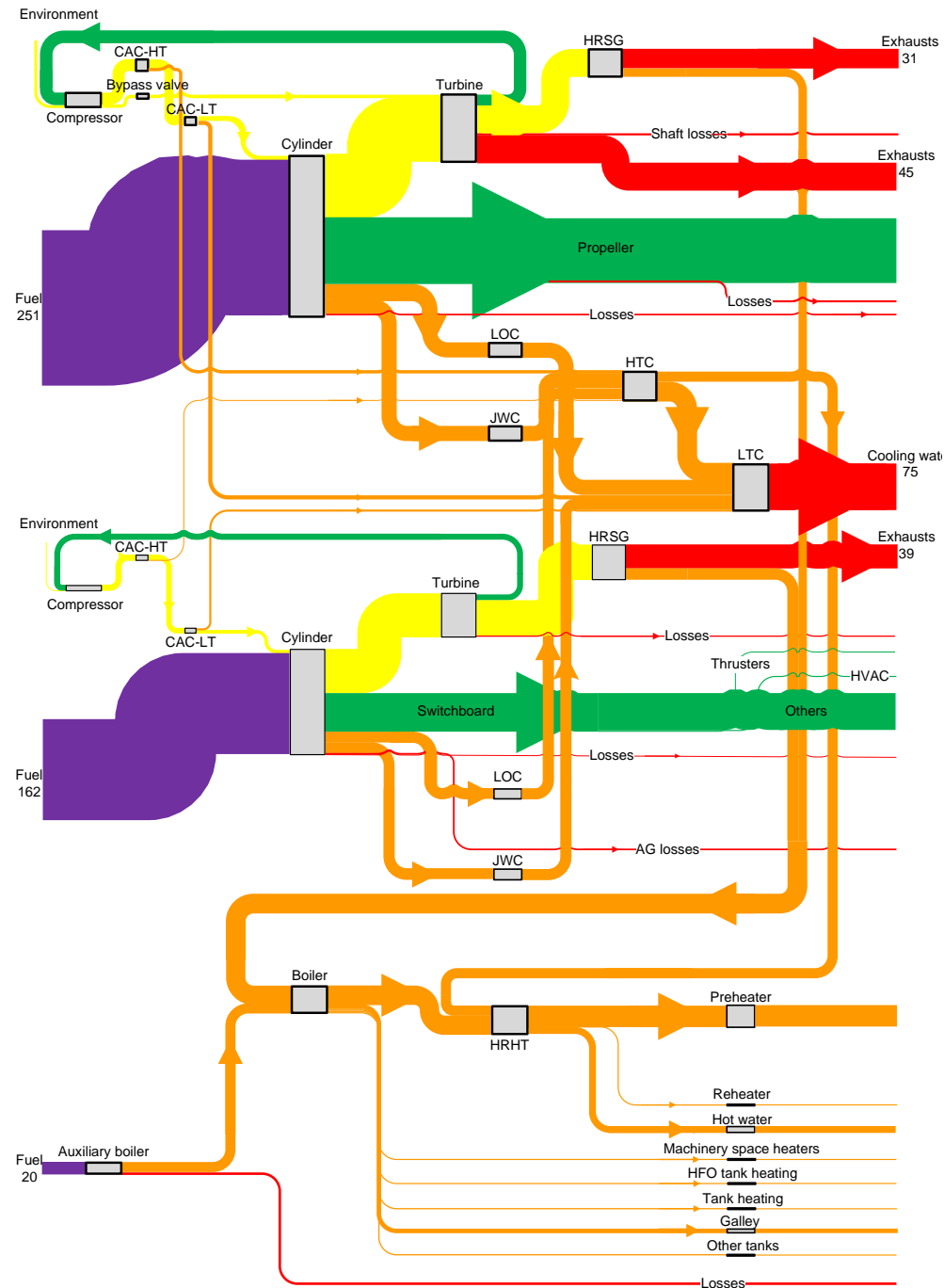


Figure 17: Sankey diagram

Component name	Contribution to exergy losses
Turbochargers	28.9%
HRSGs	10.7%
Steam heater	10.5%
HVAC preheater	10.4%
Sea water cooler	8.5%
Electric generators	6.1%

Table 1: Major contributors to ship exergy losses. Losses related to combustion are not included in the calculation

3.3. Exergy Analysis

The results of the exergy analysis of the ship energy systems are shown in Figure 18 and in Tables B.12 to B.15 in the Appendix.

It can be observed that there are large irreversibilities concentrated in some specific parts of the system that show potential for improvement. As expected, the individual largest contribution to exergy destruction in the ship systems is associated to combustion, both in the engines and in the boilers. The loss of energy resulting from the conversion of chemical energy to heat contributes to more than 76% of the total exergy destruction on board. Focusing on the remaining parts of the system, the largest sources of exergy destruction are located in the engine turbochargers (28.9%), in the exhaust gas boilers (10.7%), in the steam heater of the HTHR system (10.5%), the HVAC preheater (10.4%) and the sea water cooler (8.5%). In all the cases above, excluding the turbochargers, the exergy destruction is a consequence of a combination of large exergy flows and of the mismatch between hot and cold stream temperatures in the heat exchangers. In the exhaust boilers, exhaust gas are cooled in average from more than 300°C to 200°C, while the heat is used to generate steam at relatively low pressure (6 bar); in the steam heater, the steam is used to heat up water at 90°C; in the HVAC preheater, the relatively high-temperature water from the HTHR systems is used for heating up air to around 30°C.

From the point of view of the exergy losses, it appears that the largest exergy losses are located in the exhaust gas. It should be noted that, even though a large part of this exergy cannot be recovered given the limitations on the exhaust gas outlet temperature to avoid the condensation of sulphuric acid, there is still a significant potential to be harvested if all the available exergy in the exhaust gas was recovered. This potential is further increased

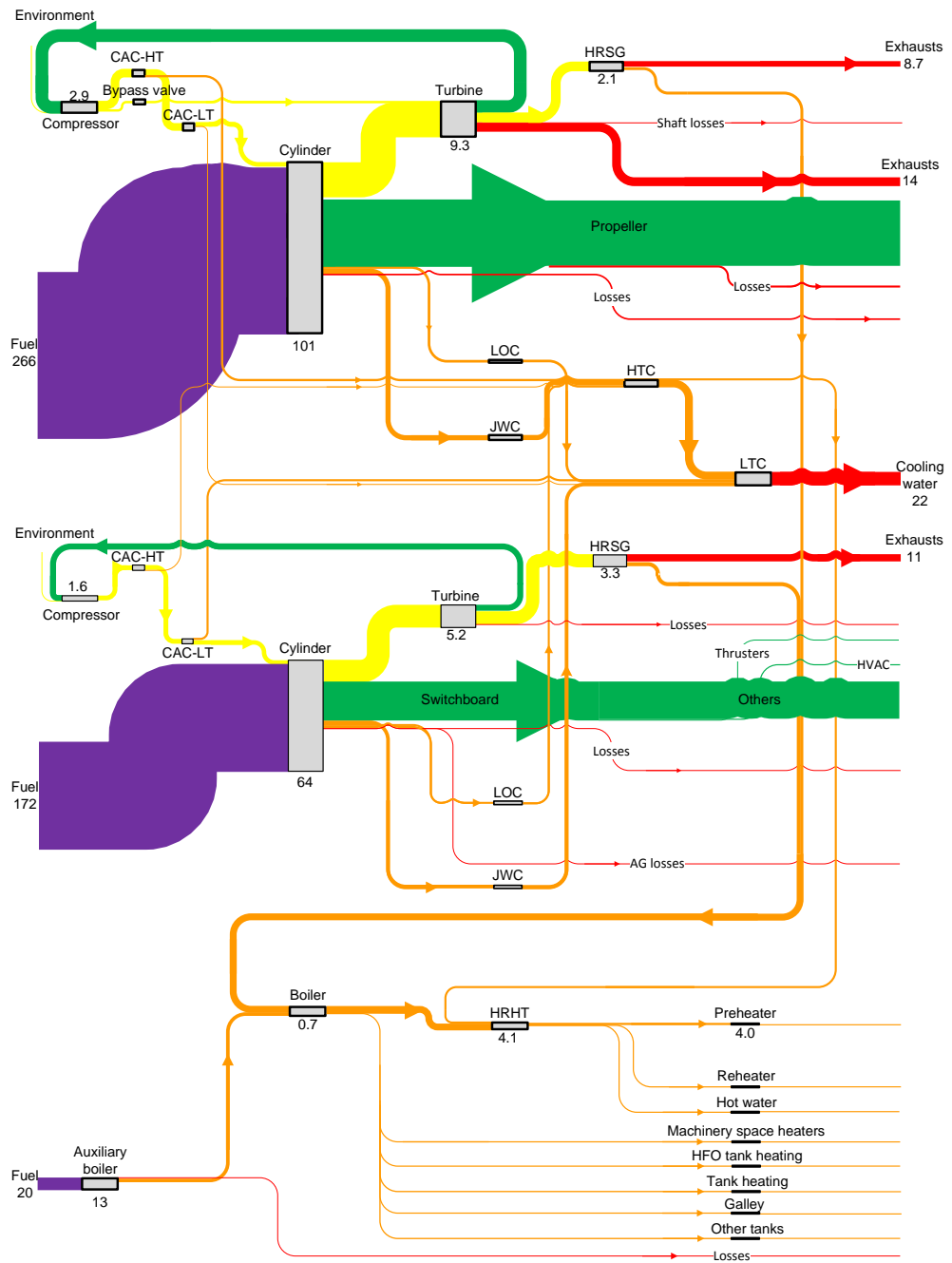


Figure 18: Grassmann diagram

by the exergy destroyed in the process of dumping steam when it is produced in excess during summer. The exergy lost in the sea water coolers as low-temperature sea water discharged to the environment is lower, highlighting the fact that the potential for improving the efficiency of the system is located in other parts of the cooling systems.

The efficiency of the recovery systems is also shown in Figure 19, where the fraction of the total energy (exergy) lost by the cooling systems and the exhaust gas of the ship's engines is represented. It can be noted that, even when only looking at the energy that can be recovered based on the existing systems (i.e. not including the LT cooling systems, for instance), the recovery efficiency is located at around 25-35% depending on whether the energy or the exergy efficiency is considered. Worth noting is also the fact that the efficiency on the exhaust gas side is lowered by the fact that two of the main engines are currently not equipped with HRSGs.

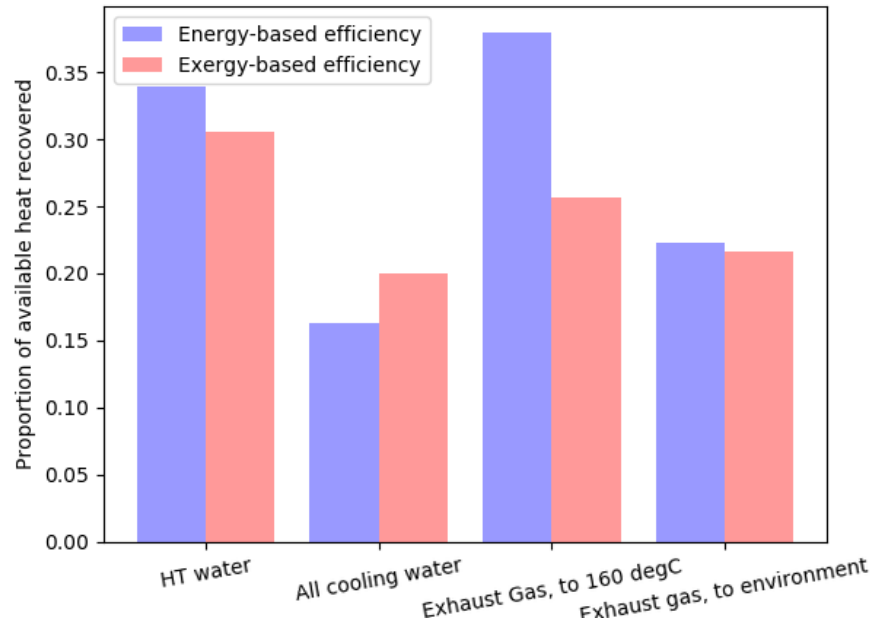


Figure 19: Energy and exergy efficiency of the WHR systems

	$P_{el} + P_{mech}$	Q_{tot}
$\sigma_{profile}$	0.65	0.10
σ_{CDC}	0.11	0.11
$ELDC$	0.23	0.07
Δ_{MLDC}	0.18	0.06
$\delta_{prod}(7\%)$	155.00	168.00

Table 2: Performance parameters for the 5-cluster power and heat

3.4. Typical operational days

A data clustering was applied at first on the total power and heating demands along the operation year, using 1000 starting points generated randomly for cluster initialization. As presented in Section 2.8, the number of typical days depends on the values of the intra- and inter-cluster distances and on the expected squared error, obeying five constraints on the load duration profiles. A higher number of typical days would result in smaller data losses, but the calculation of the ESE indicator shows that this gain of information is negligible. The average power demand is about 4700 kW with a standard deviation of 3000 kW and a 95% percentile of 8300 kW. These figures denote a high variability, but the number of optimum clusters is only 2, which shows that the power demand follows repeatable trends over time. The first typical day corresponds to more than 32000 hours (low to high demands, up to 12000 kW), and the second one to \sim 3000 hours (peak demands, above 12000 kW). On the contrary, the total heating demand presents variations of smaller amplitude, but a higher number of clusters is necessary. Five typical days appear sufficient to represent the load duration curve and energy demand profiles. The cases with the greatest power consumption and different trends are already considered in these five clusters, and the addition of an extreme period is not necessary. The large number of typical days (5) compared to those required (2) when clustering only the power demand (2) illustrates the lack of direct correlation between the power and heating requirements.

The quality of the clustering was assessed by calculating the performance indicators for both attributes (Table 2). The suggested typical periods present low relative errors and are slightly better for characterization of the heat demand profiles.

The five typical days are further segmented and the closeness of the plots

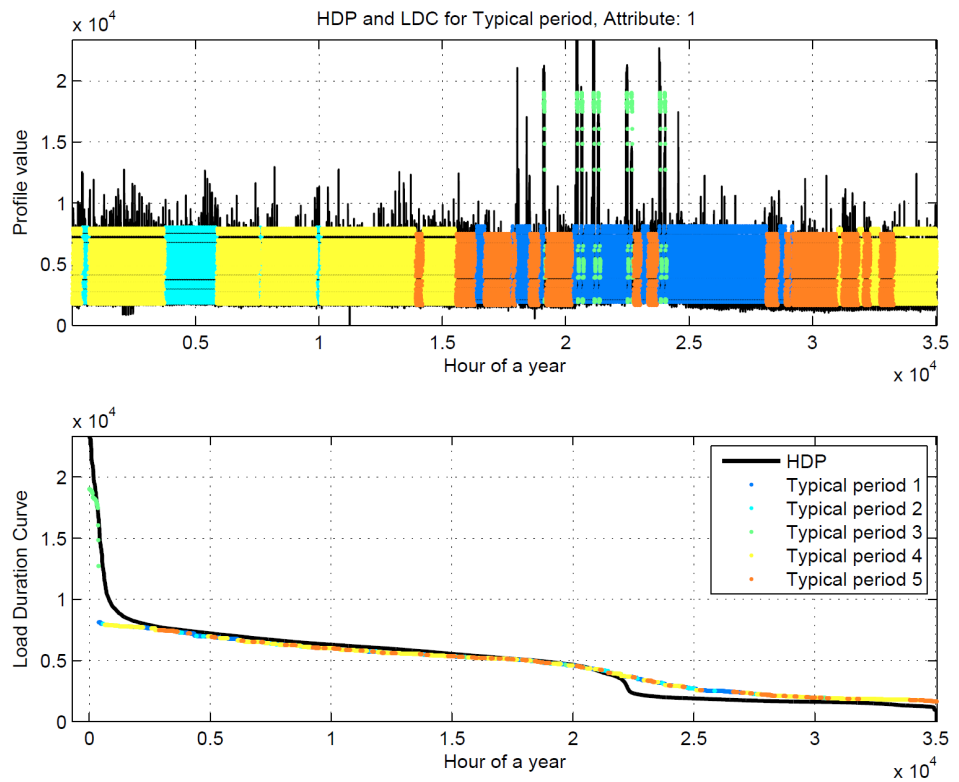


Figure 20: Power profile and duration curves, represented with the 35,040 datapoints (black curve) and five typical days (other colors).

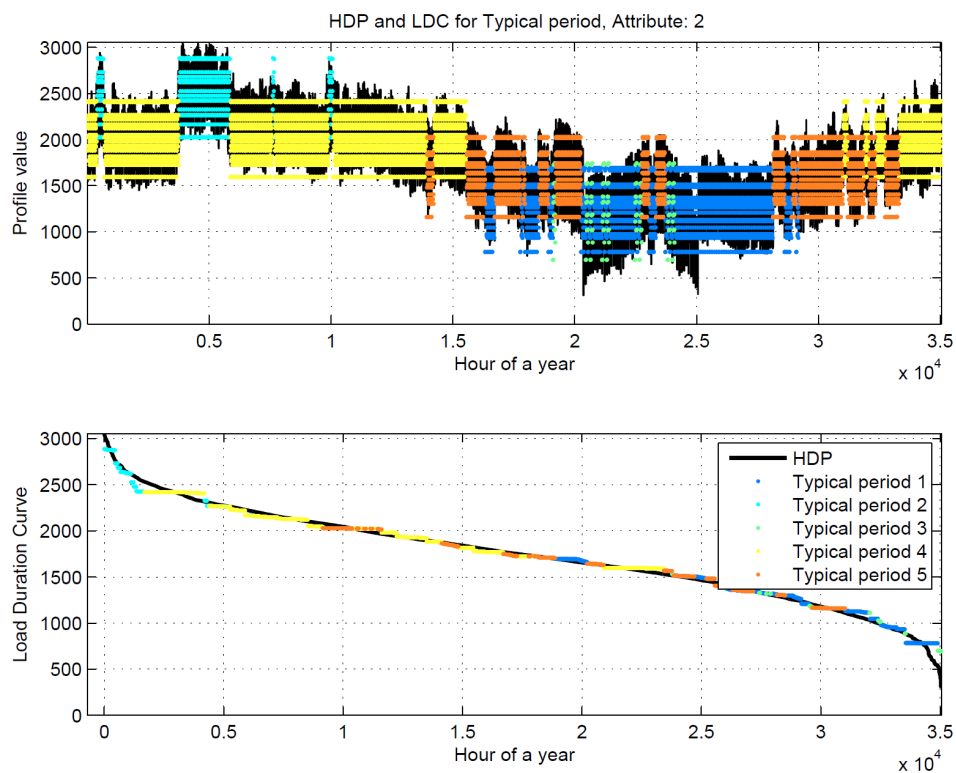


Figure 21: Power profile and duration curves, represented with the 35,040 datapoints (black curve) and five typical days (other colors).

for both demands illustrates the quality of the segmentation. In most typical days, the power consumption varies in a 2000-8000 kW range, with an average consumption of about 4500-5000 kW and similar trends. The maximum values, of about 19000 kW, are reached at highest ship speeds.

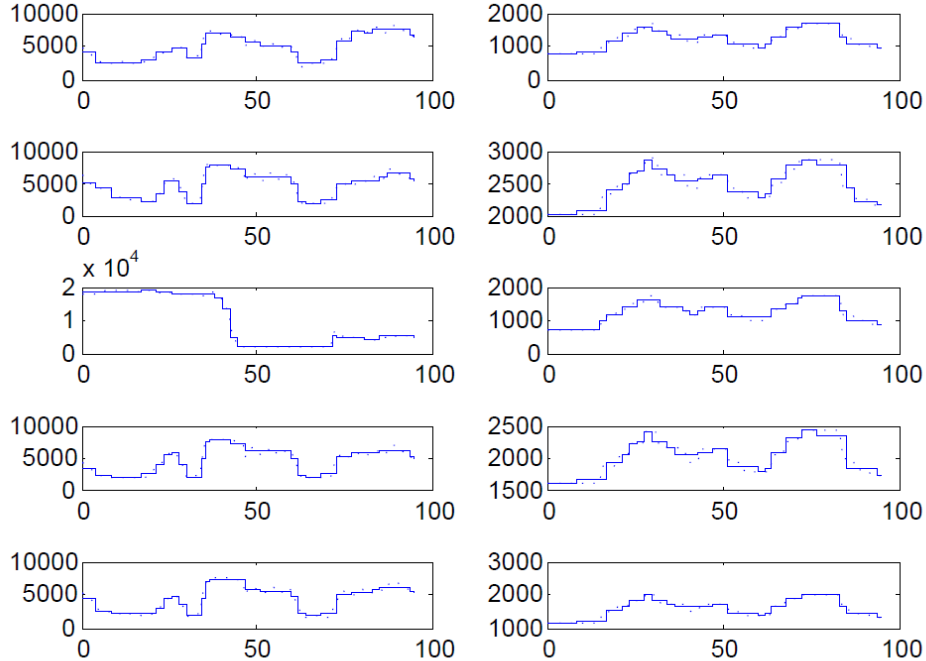


Figure 22: Power (left) and heat (right) profiles, original (dotted) and segmented (full), for the 5 typical days and duration curves.

The same findings can be deduced from the segmentation of the heat profiles as all present similar tendencies. The only significant difference is the range between the minimum and maximum values reached in a single day (e.g. 2000-2800 kW, 1000-2000 kW, 700-1700 kW, etc.). These differences are correlated to changes of the outer temperature and are thus seasonal variations. Heat storage from low-demand to high-demand days is not feasible, but may be implemented, if responsive enough, on single days.

A data clustering was applied on the total power demand and exergy destruction, following the same approach as above. In this case, the optimum number of clusters resulted to be only 2, which shows the direct relation between the power consumption and exergy destruction, and, consequently,

the weak relation with the heating needs. This result is as expected, since the engines and subsequent components are responsible for the largest irreversibilities in the system. High accuracy of the clustering for even such a small number of typical days is reached, as shown, for instance, with the relative load differences (Δ_{MLDC}) are 0.18 for both power and exergy. A further segmentation of these two typical days shows that these two variables follow the same trend in both regular and extreme conditions. The data clustering shows that, for the energy system of the case study ship, it is critical to reduce the power demand or to improve the power generation system for enhancing the system performance. Such findings are valid for all types of operation days.

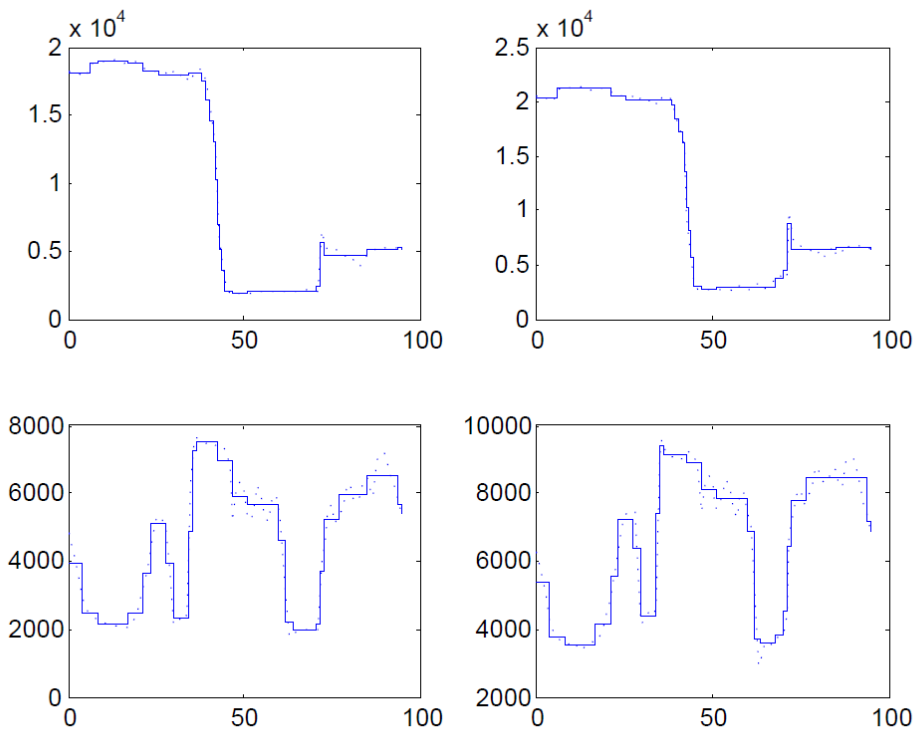


Figure 23: Exergy destruction profile and duration curve (left), represented with the 35,040 datapoints (black curve) and two typical days (dark and clear blue). Segmented power and exergy destruction profiles for the two typical days (right).

3.5. Potential for system improvement

Based on the results of the energy and exergy analysis, it is possible to identify a number of possible measures that could potentially improve the efficiency of the system.

Given the fact that many engines are operated at low load (both main and auxiliary engines), the system would benefit from both an electrification of the system and from the installation of batteries. The system electrification was explored by the authors [44] and showed a relevant potential from both an environmental and an economic point of view. The installation of batteries was also considered in a previous publication by the authors [45] and proved the potential for yearly savings of 1-2%. In this second case, however, it should be noted that the economic performance was not evaluated quantitatively.

The availability of waste heat that is not already recovered by the system suggests that the system could benefit from the installation of a Heat-to-power WHR. This possibility was tested by the authors both in the case that no additional retrofit is performed [26, 46], with estimated savings of 22% of the auxiliary power demand for a reference voyage, and in the case of a full integration with the rest of the system [45], with estimated savings of up to 6% of the total fuel consumption for a year of ship operations.

It should be noted that in the second case the advantages in terms of system performance were obtained through a system-wide optimization of the system, where an improved utilization of the low-temperature waste heat available allowed "freeing" part of the high-temperature heat from the exhaust gas to the heat-to-power WHR system, hence improving the overall exergy efficiency of the system. This includes, for instance, the concept of using heat from the LT cooling systems (currently unused) for the HVAC preheater, hence reducing exergy destruction in the HVAC preheater itself and in the steam heater. This concept could be extended to other low-temperature heat consumers (such as the machinery space heating), but it would clearly constitute a larger benefit if applied to the HVAC preheater, which is the largest heat demand on board.

The analysis also suggests that the electric power demand resulting from the use of the HVAC on board is relatively low, a consequence of the fact that the case study ship mostly operates in cold climates. This suggests that demand-related efforts should be focused on other consumers (e.g. lighting) rather than on the HVAC compressor. Also, the analysis suggests that the

use of related systems for WHR, such as absorption chillers, would not be particularly beneficial in the specific case here studied.

4. Conclusion

Shipping, similarly to any other industry, is facing challenges in relation to its contribution to climate change. In this context, cruise ships are particularly under scrutiny because of their large impact on the environment, and on their direct connection to their final users.

In this paper, we analyzed the energy system of a cruise ship operating in the Baltic Sea, with the aim of providing a better understanding of how energy is used on board, for what purposes, and with what efficiency. Although these numbers can vary substantially depending on the ship type, size and operating region, the results presented in this paper represent a unique contribution to scientific literature in terms of the detail of the analysis and of the extent of the data available.

The results showed that propulsion represents the largest share of the energy demand, as in most ships, but it is less dominant compared to other ship types, as it represents 45% of the yearly energy demand. Auxiliary electric power and heat represent an approximately equal share of the remaining part (27% and 28% respectively), with the largest share of the latter being related to space heating. This is a consequence of the ship being operated in the North of Europe, and results are expected to vary substantially for a ship operating in warmer climates (Mediterranean or Caribbean Sea, for instance).

The application of exergy analysis allowed the identification of the main causes for losses of energy quality. In addition to the combustion processes in the main engines and in the boilers, that together contribute to 77% of the exergy destruction on board, the main potential for improvement was identified in the turbochargers, the exhaust gas boilers (HRSGs), the steam heater in the hot water heat recovery systems, in the HVAC pre-heater and in the sea water cooler. The main basic causes of exergy destruction are hence to be considered the low-load operations of the engines and the mismatch in the operating temperatures of the heat exchangers.

The existing ship systems proved to have a high efficiency, at least in relation to other ships of different types. From the results of the energy and exergy analysis it can be concluded that the existing systems already

make use of a large share of the waste heat, including that at relatively low temperature that is transferred to the HT cooling systems.

Despite its good efficiency, the system shows potential for improvement. The fact that both main and auxiliary engines are operated at low load can be compensated with a higher level of electrification of the system, and by the use of batteries. The installation of an ORC can be a solution to use the high-temperature heat of the exhaust gas of the Diesel engines, while low-temperature heat from the Diesel engines could be used, instead of wasted to the sea water cooler, for space heating.

Appendix A. Energy system modelling

Appendix A.1. Data gathering and pre-processing

The operational data was collected on board from the ships' machine logging and surveillance system. The on board database tool exported all logging points to Excel-97 files, and due to the extensive amount of data points the export was divided in to 15 individual Excel-files consisting of a total 665 MB. The exported raw-data from the ship was over a time span of a full year and in most data-points in 15-min average. The Excel-files were processed in the Pandas library which is a high performance data analysis tool in Python [47]. A new structured naming of headers and a consistent time frequency over all data points were created, and 245 selected data points were saved in a HDF5 table time series database which is the base for the analysis.

All data-points were checked individually by creating a descriptive statistic and a histogram of each data-point. A filter was applied by setting up a pre-defined maximum and minimum value. As we do not know, or had any meaningful way of deriving, each individual sensors placement, sensor type or calibration status all data must be filtered and checked accordingly for outliers or bad data.

Since measurements of ambient and seawater temperature from onboard logging systems were not available for the whole dataset, we used measurements taken from SMHI database for Landsort lighthouse for the seawater, and the lighthouse Svenska Högarna for the ambient temperature. The Landsord lighthouse is situated south of the Stockholm archipelago, and the Svenska Högarna lighthouse is along the ship route, in between the Swedish archipelago and land. The assumption was validated based on June–December period, for which onboard measurements were available. This re-

sulted in a root mean square error of 1.5 K and 1.9 K for the seawater and the ambient temperature respectively, which we considered to be accurate enough for the purpose of this work. The fit the SMHI-data with the rest of the data-set the SMHI data was resampled from 1h for the seawater and 3h for the ambient temperature, to 15min frequency using a linear interpolation.

Appendix A.2. Engine modelling, figures and tables

The validity of this assumption can be seen by observing Figures A.24 and A.25 where the calculated power from the main engines is represented against the ship speed and the turbocharger speed, respectively.

$$\dot{m}_{air,comp} = \dot{m}_{air,cyl} + \dot{m}_{air,bp} \quad (\text{A.1})$$

$$\dot{m}_{eg,turb} = \dot{m}_{eg,cyl} + \dot{m}_{air,bp} \quad (\text{A.2})$$

$$\dot{m}_{eg,cyl} = \dot{m}_{air,cyl} + \dot{m}_{fuel,cyl} \quad (\text{A.3})$$

$$\dot{m}_{air,comp}\Delta h_{comp} = \dot{m}_{eg,turb}c_{p,eg}(T_{turb,in} - T_{turb,out})\eta_{mech} \quad (\text{A.4})$$

$$\dot{m}_{eg,turb}c_{p,eg}(T_{turb,in} - T_0) = \dot{m}_{air,bp}c_{p,air}(T_{comp,out} - T_0) + \dot{m}_{eg,cyl}c_{p,eg}(T_{cyl,out} - T_0) \quad (\text{A.5})$$

Where equations A.1 to A.3 represent the mass balances of the bypass split, bypass merge, and cylinder respectively, while equations A.4 and A.5 represent the energy balances of the turbocharger and of the bypass merge, respectively.

The energy balance over the whole engine is presented in Equation A.6.

$$\dot{Q}_{fuel} + \dot{Q}_{air,in} = \dot{W}_{mech} + \dot{Q}_{eg} + \dot{Q}_{cooling} \quad (\text{A.6})$$

With:

$$\dot{Q}_{fuel} = \dot{m}_{fuel}(LHV_{fuel} + c_{p,fuel}(T_{fuel,in} - T_0)) \quad (\text{A.7})$$

$$\dot{Q}_{air,in} = \dot{m}_{air}c_{p,air}(T_{air,comp,in} - T_0) \quad (\text{A.8})$$

$$\dot{Q}_{eg} = \dot{m}_{eg}c_{p,eg}(T_{eg,TC,out} - T_0) \quad (\text{A.9})$$

$$\dot{Q}_{cooling} = \dot{Q}_{CAC,HT} + \dot{Q}_{CAC,LT} + \dot{Q}_{JWC} + \dot{Q}_{LOC} \quad (\text{A.10})$$

The value of $\dot{Q}_{cooling}$ is determined based on the balance in Equation A.6. The share between the four contributions in Equation A.10 is calculated based on the data for the heat loss to the HT and LT systems presented

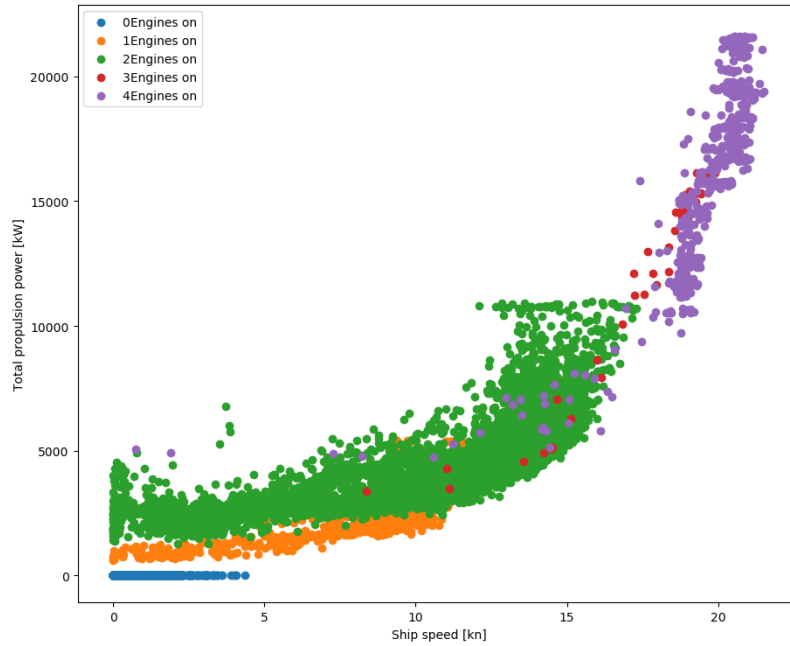


Figure A.24: Scatter plot, Propulsion power versus ship speed

in the engines project guides as functions of the engine load. The values are interpolated based on a 2^{nd} degree polynomial and scaled to respect the energy balance. In absence of more accurate data, it is then assumed that the contributions of \dot{Q}_{JWC} and \dot{Q}_{LOC} are equal for all loads.

The most relevant operative values are provided in Tables A.3 and A.4 and the main energy flows are listed in Tables A.5 and A.6.

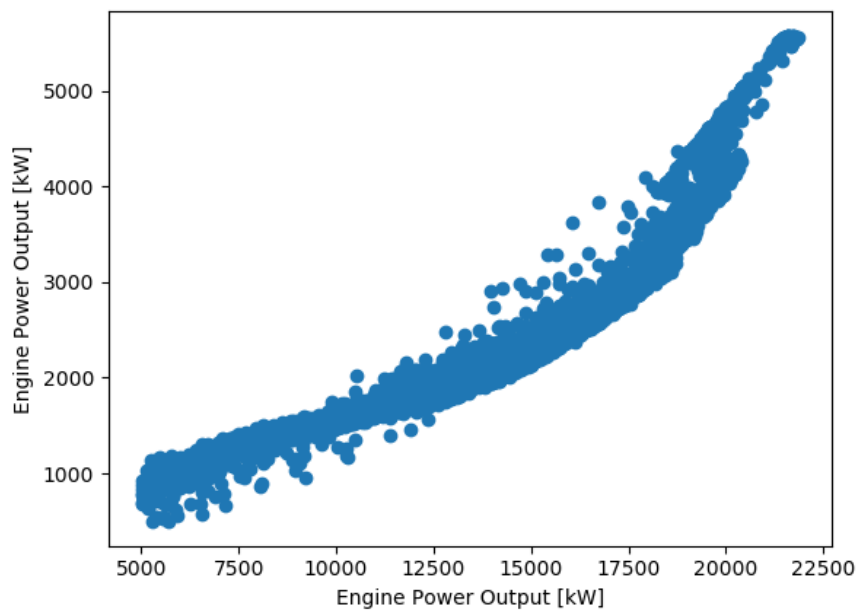


Figure A.25: Scatter plot, Main engine power versus turbocharger speed (ME1)

Variable	Unit	M/C	30%	50%	70%	90%
Compressor						
$T_{air,in}$	°C	M		302		
$T_{air,out}$	°C	C	356.0	409.4	434.1	461.7
\dot{m}_{air}	kg/s	C	4.24	7.62	8.51	10.28
β_{comp}	-	M				
Turbine						
$T_{eg,in}$	°C	C	698.8	702.2	763.3	786.0
$T_{eg,out}$	°C	M	639.3	592.9	633.2	631.0
\dot{m}_{eg}	kg/s	C	4.35	7.79	8.73	10.57
β_{exp}	-	C				
Bypass valve						
$\dot{m}_{air,BP}$	kg/s	C	0.98	2.05	1.02	0.39
Cylinders						
$\dot{m}_{air,in}$	kg/s	C	3.25	5.57	7.49	9.89
$\dot{m}_{fuel,in}$	kg/s	C	0.11	0.17	0.22	0.28
$\dot{m}_{eg,out}$	kg/s	C	3.37	5.74	7.71	10.17
$T_{air,in}$	°C	M	323.7	323.2	323.1	323.5
$T_{eg,out}$	°C	M	698.8	702.2	763.3	786.0
CAC-LT stage						
$T_{air,in}$	°C	C	355.2	350.1	360.0	368.7
$T_{air,out}$	°C	M	323.7	323.2	323.1	323.5
$T_{w,in}$	°C	M	309.3	309.6	309.5	309.6
$T_{w,out}$	°C	C	310.4	311.0	311.8	313.0
$\dot{m}_{w,LT}$	kg/s	C	23.36	26.09	29.1	31.53
CAC-HT stage						
$T_{air,in}$	°C	C	356.0	409.4	434.1	461.7
$T_{air,out}$	°C	C	355.2	350.1	360.0	368.7
$T_{w,in}$	°C	C	360.8	360.2	359.6	358.7
$T_{w,out}$	°C	C	360.8	362.6	363.6	365.4
$\dot{m}_{w,HT}$	kg/s	C	33.21	33.18	33.33	33.33
LOC						
$T_{lo,in}$	°C	C	346.6	348.9	349.8	350.5
$T_{lo,out}$	°C	M	335.1	336.8	338.1	338.3
$T_{w,in}$	°C	C	310.4	311.0	311.8	313.0
$T_{w,out}$	°C	C	317.4	317.6	317.5	318.5
JWC						
T_{wall}	°C	C		423		
$T_{w,in}$	°C	M	358.1	358.4	357.6	356.4
$T_{w,out}$	°C	C	360.8	360.2	359.6	358.7

Table A.3: Main engines, measured and calculated temperatures and flows at different engine loads

Variable	Unit	M/C	30%	50%	70%	90%
Compressor						
$T_{air,in}$	°C	M	284.2	285.3	284.9	294.6
$T_{air,out}$	°C	C	323.2	357.9	391.6	430.9
\dot{m}_{air}	kg/s	C	1.96	2.65	3.5	4.27
β_{comp}	-	M				
Turbine						
$T_{eg,in}$	°C	M	729.5	762.1	770.3	798.5
$T_{eg,out}$	°C	M	652.8	667.8	654.2	659.4
\dot{m}_{eg}	kg/s	C	2.02	2.74	3.61	4.41
β_{exp}	-	C				
Cylinders						
$\dot{m}_{air,in}$	kg/s	C	1.96	2.65	3.5	4.27
$\dot{m}_{fuel,in}$	kg/s	C	0.05	0.08	0.11	0.14
$\dot{m}_{eg,out}$	kg/s	C	2.02	2.74	3.61	4.41
$T_{air,in}$	°C	M	320.8	322.3	327.6	329.1
$T_{eg,out}$	°C	C	729.5	762.1	770.3	798.5
CAC-LT stage						
$T_{air,in}$	°C	C	323.2	356.3	366.7	372.0
$T_{air,out}$	°C	M	320.8	322.3	327.6	329.1
$T_{w,in}$	°C	M	317.1	316.3	317.5	314.1
$T_{w,out}$	°C	C	317.2	318.2	320.5	318.3
$\dot{m}_{w,LT}$	kg/s	C	11.16	11.16	10.98	10.78
CAC-HT stage						
$T_{air,in}$	°C	C	323.2	357.9	391.6	430.9
$T_{air,out}$	°C	C	323.2	356.3	366.7	372.0
$T_{w,in}$	°C	C	362.5	364.2	368.0	368.2
$T_{w,out}$	°C	C	362.5	364.3	369.3	371.9
$\dot{m}_{w,HT}$	kg/s	C	16.66	16.67	16.55	16.67
LOC						
$T_{lo,in}$	°C	C	348.2	350.3	354.0	357.3
$T_{lo,out}$	°C	M	336.6	337.4	339.7	340.4
$T_{w,in}$	°C	C	317.2	318.2	320.5	318.3
$T_{w,out}$	°C	C	325.9	327.8	331.4	331.3
JWC						
T_{wall}	°C	C		423		
$T_{w,in}$	°C	M	360.0	359.7	362.3	361.5
$T_{w,out}$	°C	C	362.5	364.2	368.0	368.2

Table A.4: Auxiliary engines, measured and calculated temperatures and flows at different engine loads

Energy flow	type	30%	50%	70%	90%
Power output	Mech	1767	2946	4118	5293
Exhaust gas (after turbine)	Heat	1672	2566	3227	3938
CAC-LT	Heat	80	197	353	613
CAC-HT	Heat	0	256	470	763
JWC	Heat	501	507	549	620
LOC	Heat	501	507	549	620

Table A.5: Main engines, energy flows at different engine loads

Energy flow	type	30%	50%	70%	90%
Power output	Mech	828	1381	1932	2482
Exhaust gas (after turbine)	Heat	808	1144	1456	1753
CAC-LT	Heat	5	92	139	185
CAC-HT	Heat	0	4	87	256
JWC	Heat	278	366	436	510
LOC	Heat	278	366	436	510

Table A.6: Auxiliary engines, energy flows at different engine loads

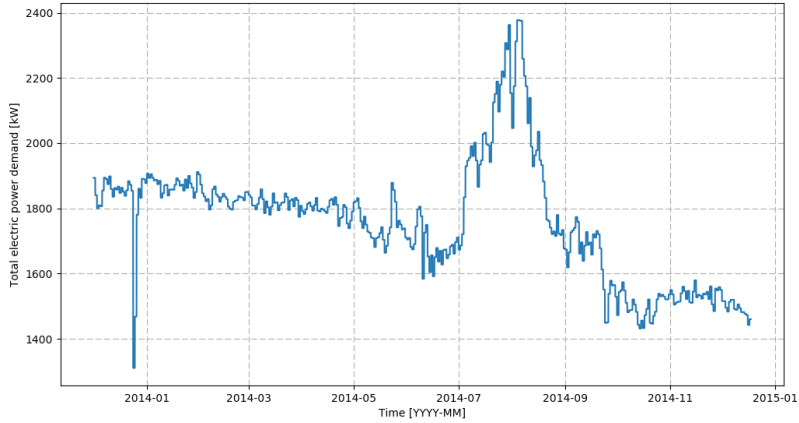


Figure A.26: Total electric power demand versus time (Daily average)

Appendix A.3. Electric demand modelling

Appendix A.3.1. HVAC systems

The observation of the total power demand over the year (see Figure A.26, showing daily averages) leads to the identification of a period, corresponding to the summer months, when the electric power demand is significantly higher than during the remaining months. Based on this observation, in this work we assumed that the demand of the HVAC compressors related to the need for space cooling is concentrated during the summer months. Additionally, comparing the evolution of the daily demand (see Figure A.27, representing the instantaneous demand divided by the daily average) between a typical summer and winter day, shows that the daily variation is comparable. This shows that assuming a constant consumption for the HVAC during the day does not introduce a substantial error in the estimations.

Hence, the HVAC electric power demand was estimated as follows:

$$P_{el,HVAC} = \begin{cases} P_{el,tot}(t) - P_{el,ref}(t), & \text{if } 2014-07-03 < t < 2014-08-21 \\ 0, & \text{otherwise} \end{cases} \quad (\text{A.11})$$

where $P_{el,ref}(t)$ is calculated as:

$$P_{el,ref}(t) = 0.5(P_{el,tot}(t_1) + P_{el,tot}(t_2)) \quad (\text{A.12})$$

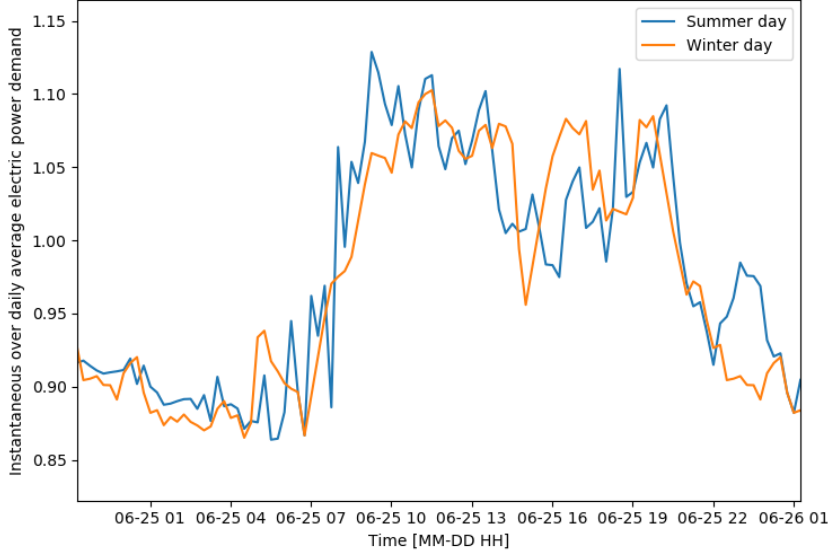


Figure A.27: Instantaneous power demand over daily average, winter versus summer day

Appendix A.3.2. Thrusters

When entering port areas, the ship needs to use thrusters to maneuver and berth. In the case of this particular ships, operating on daily schedules and hence maneuvering four times per day, the power demand related to thrusters can be significant. In order to isolate the demand from the thrusters, we extracted from ship operations a reference daily energy profile, based on the instantaneous electric power demand divided by the daily average. From this daily profile (made of 96 points), we manually selected the points that could be clearly identified as related to the thrusters energy demand, and substituted the actual value with a weighted average of the previous and subsequent points (see Figure A.28).

By comparing the reference profile to the instantaneous one, the points where the former is more than 10% higher than the latter are identified as "thruster-on" points and treated consequently.

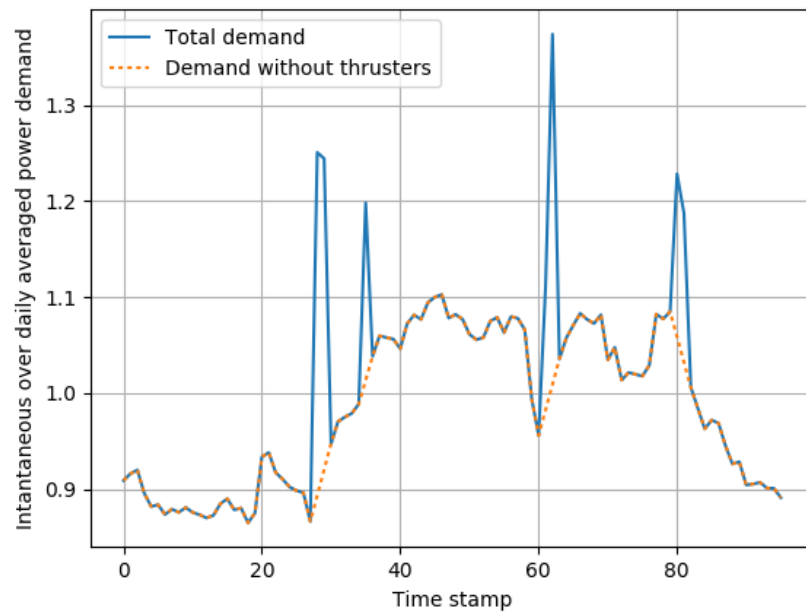


Figure A.28: Example of the procedure of selection of thruster power demand

Appendix A.3.3. Heat balance parameter estimation

The individual contributions of different consumers were determined by means of a parameter estimation procedure, using the daily boiler fuel consumption for the calibration of the parameters. The parameter estimation problem is hence written as a minimization problem:

$$\min \quad \left(\frac{\sum_i (y(\mathbf{p}) - \bar{y})^2}{\sum_i \bar{y}^2} \right)^{0.5} \quad (\text{A.13})$$

$$(\text{A.14})$$

where the vector \mathbf{p} includes the calibration parameters that are part of the heat demand and generation estimation model that is explained in detail in the following sections. A list of the parameters \mathbf{p} is shown in Table A.7, together with the chosen upper and lower boundaries for the calibration procedure.

Appendix A.3.4. Heat demand

The heat demand was calculated as the sum of the contributions of the elements listed in the ship's heat balance documentation. The assumptions used in the estimation are summarized in Table A.8:

where all f_i factors are treated as calibration parameters (see table A.7). The $\Phi_G(\hat{t})$ and $\Phi_{HWH}(\hat{t})$ functions represent the assumption made on the daily evolution of the heating demand from the galley and the hot water heater respectively. The daily evolutions of the demand are considered to be the same over the whole year of operations and are represented graphically in Figure A.29.

Appendix A.3.5. Heat generation

The heat recovered in the EGBs is the only contribution to the heat balance that is known with a reasonable certainty. The heat transferred from the exhaust gas to the steam (\dot{Q}_{EGB}) is calculated according to equation Appendix A.3.5:

$$\dot{Q}_{EGB} = \dot{m}_{eg} c_{p,eg} (T_{eg,EGB,in} - T_{eg,EGB,out}) \quad (\text{A.15})$$

where $T_{eg,EGB,out}$ and $T_{eg,EGB,in}$ are measured for all EGBs, $c_{p,eg}$ is calculated as a function of the exhaust gas composition and temperature, and \dot{m}_{eg} is calculated based on the engine energy and mass balance.

Parameter name	Symbol	Unit	Lower Bound- ary	Higher Bound- ary	Optimal value
Constant HTHR heat demand	$\dot{Q}_{k,HTHR}$	kW	0	1000	20.5
Constant steam demand	$\dot{Q}_{k,steam}$	kW	0	1000	0
Weight factor of the HVAC Re-heater	$f_{HVAC,RH}$	-	0.5	1	0.40
Weight factor of the HVAC Pre-heater	$f_{HVAC,PH}$	-	0	1	1.00
Weight factor of hot water heater	f_{HWH}	-	0.5	1	0.72
Weight factor of the galley	f_G	-	0.5	1	0.68
Weight factor of the other consumers	f_{Other}	-	0.5	1	0.21
HTHR inlet temperature	$T_{HTHR,ER1,in}$	K	343	353	348
Effectiveness of the HTHR HEX	ϵ_{HTHR}	-	0.5	0.9	0.5
Boiler drum steam storage capacity	$Q_{ab,max}$	MJ	100	100000	9.5e6
Boiler heat rate	$\dot{Q}_{ab,des}$	kW	2000	8000	5100

Table A.7: Parameters optimized in the parameter estimation for the heat balance

Heat flow name		Equation
HVAC	Pre-heater	$\dot{Q}_{HVAC,PH} = f_{HVAC,RH} \dot{Q}_{HVAC,PH,des} \frac{\dot{W}_{HVAC}(t)}{\dot{W}_{HVAC,max}}$
HVAC	Re-heater	$\dot{Q}_{HVAC,RH} = f_{HVAC,PH} \dot{Q}_{HVAC,PH,des} \frac{T_{in} - T_{air,out}(t)}{T_{in} - T_{air,out,des}}$
Hot water heater		$\dot{Q}_{HWH} = f_{HWH} \dot{Q}_{HWH,des} \Phi_{HWH}(\hat{t})$
Galley		$\dot{Q}_G = f_G \dot{Q}_{G,des} \Phi_G(\hat{t})$
Low temperature tank heating		$\dot{Q}_{TH} = f_{TH} \dot{Q}_{TH} \frac{T_T - T_{air,out}(t)}{T_T - T_{air,out,des}}$
HFO tank heating		$\dot{Q}_{HTH} = f_{HTH} \dot{Q}_{HTH} \frac{T_{HT} - T_{air,out}(t)}{T_{HT} - T_{air,out,des}}$
Machinery space heating		$\dot{Q}_{MSH} = f_{MSH} \dot{Q}_{MSH} \frac{T_{MS} - T_{air,out}(t)}{T_{MS} - T_{air,out,des}}$
HFO heater		$\dot{Q}_{HH} = \dot{m}_{HFO}(t) c_{p,HFO} (T_{HFO,inj} - T_{HT})$

Table A.8: Summary of the heat demand contributions and their calculation

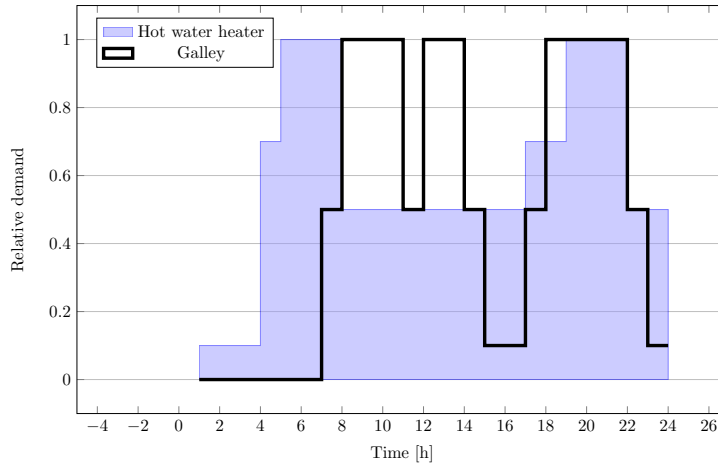


Figure A.29: Hourly relative demand of hot water heating and galley

It is known that the ship heating systems are designed for recovering energy from the high temperature cooling systems of all the ship's engines. Based on the available measurements, we calculated the heat exchanged in the two HTHRs according to equation A.17,

$$\begin{aligned}\dot{Q}_{HTHR} &= \dot{Q}_{HTHR,ER1} + \dot{Q}_{HTHR,ER2} \\ &= \sum_{i=ER1,ER2} \epsilon_{HTHR} * \dot{m}_{min,HTHR,i} * c_{p,w} * (T_{HT,out,i} - T_{HRH,ER,in})\end{aligned}\quad (\text{A.16})$$

where the effectiveness of the heat exchanger ϵ_{HTHR} is considered to be constant and its value is part of the parameter estimation problem (see table A.7). The HT water outlet temperature for each engine room is calculated based on the thermal balance of the engines, and the HR water at the HTHR inlet ($T_{HRH,ER,in}$) is considered as a calibration parameter.

The heat generated by the auxiliary boilers is calculated as to close the heat balance of the ship energy systems. The contribution of the boiler heat storage capacity is taken into account by a calibration parameter $Q_{ab,max}$ that determines the maximum heat deficit. This corresponds, in practice, to assuming that the boiler is started up when the steam pressure inside the boiler drops below a certain value, and stopped once the pressure has achieved its maximum operative value. In this calculation, the calibration parameters are the heat storage capacity ($Q_{ab,max}$) and the fixed heat rate ($\dot{Q}_{ab,des}$) of the auxiliary boilers (see table A.7).

Appendix A.3.6. Parameter estimation and uncertainty quantification

In this study, we base the estimation of the uncertainty on the production side, as it is the one that has the largest amount of information available. In these regards, the uncertainty can be reduced to the contribution of three elements: $U(\dot{Q}_{EGB})$, $U(\dot{Q}_{HTHR})$, $U(\dot{Q}_{AB})$.

The uncertainty on the heat generated in the EGBs can be further subdivided based on its definition as a composition of the uncertainty of $T_{eg,EGB,in}$, $T_{eg,EGB,out}$, \dot{m}_{eg} , and $c_{p,eg}$. In the case of $T_{eg,EGB,in}$ and $T_{eg,EGB,out}$, measured values are used, where the uncertainty is related to the sensors (K-type thermocouples) that can be as high as 4% [CIT]. The uncertainty on the \dot{m}_{eg} is related to the calculation assumptions and can be estimated of being up to 10%. The uncertainty of the $c_{p,eg}$ value, given that both composition and temperature are accounted for, should be within 5% of the reference value.

These assumptions lead to the following estimation of the uncertainty:

$$\frac{\delta \dot{Q}_{gen}}{\dot{Q}_{gen}} = \sqrt{\frac{\delta \dot{m}_{eg}^2}{\dot{m}_{eg}^2} + \frac{\delta c_{p,eg}^2}{c_{p,eg}^2} + \frac{\delta T_{EGB,in}^2 + \delta T_{EGB,out}^2}{(T_{EGB,in} - T_{EGB,out})^2}} \quad (\text{A.18})$$

That once typical values are assigned can be as high as 30%, where most of the variability is related to the temperature measurements.

The uncertainty of the heat generated by the ABs can be reduced to the contribution of two elements: the uncertainty on $\dot{m}_{fuel,AB}$ and that on η_{AB} . The former will be at least as large as the calibration error (35%) and will be considered equal to 50% to be conservative and accounting also for errors in the aggregated boiler fuel measurements. In addition, the uncertainty on the efficiency can be considered to be around 10% based on the discrepancy between the considered sources and on the expected variability of the efficiency with load. Similarly to the previous case, the combination of these efficiencies lead to a total uncertainty of 51%, where the main contribution comes from the uncertainty of the model output compared to the actual fuel consumption.

The estimation of the uncertainty of \dot{Q}_{HTHR} can be based on A.17 having assigned an acceptable variation of 20% to the effectiveness of the heat exchanger, 20% on the estimation of the reference mass flow, ± 5 K uncertainty on water temperature measurements and considering negligible the uncertainty on $c_{p,w}$, leading to a 145% uncertainty on this measurement.

Appendix B. Full tables of energy and exergy flows

Appendix B.1. Energy flows

	From	To	Type	Total	P/S	LSS	Man	HSS	Win	Mid	Sum	
E	Env.	ME	Comp.	Ph	4.57	0.005	3.819	0.385	0.359	2.327	1.671	0.571
ME	Comp.	ME	CAC-HT	Ph	19.27	0.010	14.412	1.645	3.208	7.494	7.822	3.958
ME	CAC-HT	ME	CAC-LT	Ph	13.98	0.010	10.900	1.190	1.885	5.717	5.728	2.541
ME	CAC-LT	ME	Cyl.	Ph	7.35	0.009	5.951	0.655	0.737	3.340	2.969	1.043
ME	Turb.	ME	Comp.	W	20.16	0.006	15.287	1.659	3.207	7.539	8.523	4.098
ME	Cyl.	ME	Turb.	Ph	103.85	0.093	82.544	9.285	11.924	41.276	43.973	18.597
ME	Turb.	E	HRSG	Ph	44.77	0.044	36.434	3.974	4.318	18.383	18.840	7.546
ME	Turb.	E	Losses	Q	3.32	0.003	2.652	0.289	0.378	1.307	1.425	0.590
ME	Comp.	ME	BP valve	Ph	24.73	0.011	19.106	2.045	3.567	9.866	10.194	4.669
ME	Bypass valve	ME	Turb.	Ph	5.45	0.002	4.694	0.399	0.359	2.372	2.372	0.711
ME	CAC-HT	CS	HT Cool.	Q	5.29	0.000	3.512	0.455	1.323	1.778	2.094	1.418
ME	CAC-LT	CS	LT Cool.	Q	6.63	0.001	4.949	0.535	1.147	2.377	2.758	1.497
ME	Cyl.	ME	LOC	Q	24.36	0.067	19.869	2.665	1.763	9.835	10.735	3.793
ME	Cyl.	ME	JWC	Q	24.36	0.067	19.869	2.665	1.763	9.835	10.735	3.793
ME	JWC	CS	HT Cool.	Q	24.36	0.067	19.869	2.665	1.763	9.835	10.735	3.793
ME	LOC	CS	LT Cool.	Q	24.36	0.067	19.869	2.665	1.763	9.835	10.735	3.793
ME	Cyl.	E	Losses	Q	2.59	0.007	2.133	0.280	0.172	1.054	1.143	0.396
ME	HRSG	S	Boiler	Q	13.41	0.018	11.130	1.277	0.987	5.810	5.439	2.163
ME	HRSG	E	Env.	Ph	31.36	0.025	25.304	2.697	3.331	12.573	13.402	5.383
ME	Cyl.	P	Prop. sh.	W	107.39	0.141	85.158	10.141	11.947	42.238	45.916	19.233
ME	Fuel tank	ME	Cyl.	Chl	250.62	0.360	199.949	23.977	26.331	99.059	107.585	43.973
ME	Fuel tank	ME	Cyl.	Q	1.09	0.002	0.875	0.102	0.109	0.455	0.458	0.174

Table B.9: Summary of energy flows for the main engines

From	To	Type	Total	P/S	LSS	Man	HSS	Win	Mid	Sum
E Env.	AE Comp.	Ph	0.42	0.13	0.23	0.05	0.01	0.25	0.09	0.08
AE Comp.	AE CAC-HT	Ph	9.96	3.64	5.08	0.89	0.35	4.34	3.85	1.76
AE CAC-HT	AE CAC-LT	Ph	8.91	3.13	4.68	0.83	0.27	3.99	3.54	1.38
AE CAC-LT	AE Cyl.	Ph	5.62	1.76	3.13	0.59	0.14	2.75	2.20	0.67
AE Turb.	AE Comp.	W	9.54	3.50	4.85	0.84	0.34	4.09	3.76	1.69
AE Cyl.	AE Turb.	Ph	70.69	21.90	39.33	7.46	2.00	30.33	29.78	10.57
AE Turb.	E HRSG	Ph	56.90	17.21	32.13	6.00	1.57	24.42	24.18	8.30
AE Turb.	E Losses	Q	1.89	0.54	1.05	0.25	0.05	0.80	0.82	0.27
AE Comp.	AE BP valve	Ph	9.96	3.64	5.08	0.89	0.35	4.34	3.85	1.76
AE Bypass valve	AE Turb.	Ph	0.00	0.00	0.00	0.00	0.00	0.00	0.00	0.00
AE CAC-HT	CS HT Cool.	Q	1.04	0.51	0.41	0.06	0.07	0.34	0.31	0.39
AE CAC-LT	CS LT Cool.	Q	3.29	1.37	1.55	0.24	0.13	1.24	1.34	0.70
AE Cyl.	AE LOC	Q	17.47	5.30	9.75	1.98	0.44	7.49	7.48	2.50
AE Cyl.	AE JWC	Q	17.47	5.30	9.75	1.98	0.44	7.49	7.48	2.50
AE JWC	CS HT Cool.	Q	17.47	5.30	9.75	1.98	0.44	7.49	7.48	2.50
AE LOC	CS LT Cool.	Q	17.47	5.30	9.75	1.98	0.44	7.49	7.48	2.50
AE Cyl.	E Losses	Q	1.50	0.39	0.88	0.19	0.04	0.64	0.67	0.20
AE HRSG	S Boiler	Q	18.30	5.43	10.43	1.99	0.45	8.08	7.49	2.73
AE HRSG	E Env.	Ph	38.60	11.78	21.69	4.01	1.11	16.34	16.68	5.58
AE Cyl.	EL Switchboard	W	62.02	20.78	34.33	6.25	1.85	26.97	26.34	9.89
AE Cyl.	E AG losses	Q	3.47	0.93	2.03	0.43	0.09	1.47	1.53	0.47
AE Fuel tank	AE Cyl.	Ch	162.13	51.30	89.38	16.88	4.57	68.96	68.53	24.64
AE Fuel tank	AE Cyl.	Q	0.62	0.15	0.38	0.06	0.02	0.28	0.25	0.08

Table B.10: Summary of energy flows for the auxiliary engines

From	To	Type	Total	P/S	LSS	Man	HSS	Win	Mid	Sum
CS HT Cool.	CS LT Cool.	Q	31.84	3.48	21.94	3.57	2.85	12.29	13.62	5.93
CS HT Cool.	S HRHT	Q	16.33	2.39	11.60	1.59	0.75	7.15	7.01	2.17
S Boiler	S HRHT	Q	31.06	14.15	14.50	2.15	0.26	18.16	11.25	1.66
S Aux Boiler	S Boiler	Ph	16.22	13.56	2.32	0.43	0.09	10.50	5.42	0.30
S Aux Boiler	E Env.	Ph	4.05	2.83	1.00	0.22	0.00	2.62	1.35	0.07
S Fuel Tank	S Aux Boiler	Ch	20.32	14.19	5.04	1.08	0.01	13.13	6.81	0.37
S HRHT	D Preheater	Q	34.51	12.33	19.12	2.56	0.50	21.02	13.49	0.00
S HRHT	D Reheater	Q	1.83	0.60	0.86	0.19	0.18	0.00	0.00	1.83
S HRHT	D HWH	Q	11.05	3.60	6.12	1.00	0.33	4.29	4.76	2.00
S Boiler	D MSH	Q	1.99	0.69	1.07	0.17	0.06	0.81	0.90	0.28
S Boiler	D HFO TH	Q	1.92	0.67	1.03	0.16	0.05	0.79	0.86	0.27
S Boiler	D HFO H	Q	1.29	0.16	0.90	0.13	0.10	0.52	0.55	0.21
S Boiler	D TH	Q	1.49	0.52	0.80	0.13	0.04	0.61	0.67	0.21
S Boiler	D G	Q	7.11	1.96	4.33	0.64	0.17	2.97	3.19	0.95
S Boiler	D OT	Q	1.49	0.52	0.80	0.13	0.04	0.61	0.67	0.21
EL Switchboard	EL Thrusters	W	0.94	0.00	0.00	0.94	0.00	0.36	0.43	0.15
EL Switchboard	EL HVAC	W	1.79	0.59	0.85	0.18	0.18	0.00	0.00	1.79
EL Switchboard	EL Other el. dem.	W	59.29	19.99	32.66	4.99	1.64	26.06	25.45	7.78
P Prop. sh. shaft	P Prop. sh.	W	104.19	0.14	82.62	9.84	11.59	40.98	44.55	18.66
P Prop. sh. shaft	E Losses	Q	3.20	0.00	2.54	0.30	0.36	1.26	1.37	0.57

Table B.11: Summary of energy flows for the boiler/steam systems

Appendix B.2. Exergy flows

From	To	Type	Total	P/S	LSS	Man	HSS	Win	Mid	Sum
E Env.	ME Comp.	Ph	0.16	0.000	0.141	0.013	0.010	0.102	0.048	0.014
ME Comp.	ME CAC-HT	Ph	13.64	0.004	9.932	1.148	2.555	4.976	5.626	3.037
ME CAC-HT	ME CAC-LT	Ph	12.20	0.004	9.008	1.023	2.164	4.476	5.079	2.643
ME CAC-LT	ME Cyl.	Ph	11.04	0.004	8.144	0.932	1.960	4.019	4.619	2.401
ME Turb.	ME Comp.	W	20.16	0.006	15.287	1.659	3.207	7.539	8.523	4.098
ME Cyl.	ME Turb.	Ph	55.91	0.037	43.951	4.839	7.085	22.177	23.408	10.327
ME Turb.	E HRSG	Ph	15.45	0.014	12.621	1.353	1.458	6.605	6.320	2.520
ME Turb.	E Losses	Q	0.81	0.001	0.653	0.069	0.087	0.341	0.338	0.131
ME Turb.	E Env.	Ph	14.04	0.014	11.256	1.285	1.489	5.694	5.941	2.409
ME Comp.	ME BP valve	Ph	17.44	0.004	13.179	1.425	2.831	6.557	7.323	3.559
ME BP valve	ME Turb.	Ph	3.80	0.001	3.246	0.277	0.275	1.581	1.697	0.522
ME CAC-HT	CS HT Cool.	Q	1.16	0.000	0.924	0.125	0.392	0.501	0.547	0.394
ME CAC-LT	CS LT Cool.	Q	0.59	0.000	0.864	0.091	0.203	0.456	0.460	0.242
ME Cyl.	ME LOC	Q	4.18	0.011	3.442	0.443	0.286	1.860	1.758	0.565
ME Cyl.	ME JWC	Q	8.13	0.022	6.660	0.879	0.565	3.424	3.514	1.188
ME JWC	CS HT Cool.	Q	5.30	0.022	6.660	0.879	0.565	3.424	3.514	1.188
ME LOC	CS LT Cool.	Q	2.45	0.011	3.442	0.443	0.286	1.860	1.758	0.565
ME Cyl.	E Losses	Q	0.63	0.002	0.525	0.067	0.040	0.275	0.271	0.088
ME HRSG	S Boiler	Q	4.63	0.008	5.622	0.628	0.498	3.015	2.677	1.064
ME HRSG	E Env.	Ph	8.69	0.006	6.999	0.725	0.961	3.590	3.643	1.456
ME Cyl.	P Prop. sh.	W	107.39	0.141	85.158	10.141	11.947	42.238	45.916	19.233
ME Fuel tank	ME Cyl.	Ch	266.02	0.382	212.237	25.450	27.949	105.146	114.197	46.675
ME Fuel tank	ME Cyl.	Q	0.15	0.000	0.125	0.014	0.014	0.068	0.063	0.022

Table B.12: Summary of exergy flows for the main engines

From	To	Type	Total	P/S	LSS	Man	HSS	Win	Mid	Sum
E Env.	AE Comp.	Ph	0.01	0.002	0.003	0.001	0.000	0.003	0.001	0.001
AE Comp.	AE CAC-HT	Ph	7.91	2.960	4.008	0.659	0.288	3.392	3.091	1.432
AE CAC-HT	AE CAC-LT	Ph	7.65	2.835	3.906	0.644	0.269	3.302	3.017	1.335
AE CAC-LT	AE Cyl.	Ph	7.09	2.589	3.650	0.606	0.248	3.066	2.802	1.227
AE Turb.	AE Comp.	W	9.54	3.504	4.853	0.841	0.338	4.087	3.762	1.687
AE Cyl.	AE Turb.	Ph	36.26	11.776	19.815	3.592	1.079	15.705	14.961	5.597
AE Turb.	E HRSG	Ph	21.04	6.378	11.936	2.157	0.571	9.166	8.866	3.011
AE Turb.	E Losses	Q	0.46	0.132	0.259	0.060	0.012	0.209	0.194	0.060
AE Comp.	AE BP valve	Ph	7.91	2.960	4.008	0.659	0.288	3.392	3.091	1.432
AE BP valve	AE Turb.	Ph	0.00	0.000	0.000	0.000	0.000	0.000	0.000	0.000
AE CAC-HT	CS HT Cool.	Q	0.24	0.125	0.102	0.015	0.018	0.090	0.074	0.097
AE CAC-LT	CS LT Cool.	Q	0.36	0.245	0.256	0.037	0.021	0.236	0.215	0.108
AE Cyl.	AE LOC	Q	3.14	0.962	1.757	0.344	0.075	1.476	1.275	0.388
AE Cyl.	AE JWC	Q	5.84	1.772	3.270	0.656	0.144	2.608	2.451	0.783
AE JWC	CS HT Cool.	Q	3.90	1.772	3.270	0.656	0.144	2.608	2.451	0.783
AE LOC	CS LT Cool.	Q	2.18	0.962	1.757	0.344	0.075	1.476	1.275	0.388
AE Cyl.	E Losses	Q	0.37	0.096	0.217	0.047	0.008	0.166	0.159	0.044
AE HRSG	S Boiler	Q	6.32	2.869	5.504	1.011	0.237	4.309	3.901	1.412
AE HRSG	E Env.	Ph	11.42	3.509	6.432	1.145	0.334	4.857	4.965	1.599
AE Cyl.	EL SB	W	62.02	20.781	34.328	6.249	1.851	26.971	26.344	9.894
AE Cyl.	E AG losses	Q	0.85	0.228	0.499	0.105	0.020	0.384	0.363	0.104
AE Fuel tank	AE Cyl.	Ch	172.09	54.452	94.876	17.916	4.849	73.199	72.744	26.150
AE Fuel tank	AE Cyl.	Q	0.08	0.019	0.054	0.009	0.003	0.041	0.033	0.010

Table B.13: Summary of exergy flows for the auxiliary engines

From	To	Type	Total	P/S	LSS	Man	HSS	Win	Mid	Sum
CS HT Cool.	CS LT Cool.	Q	7.36	1.46	8.63	1.36	0.97	5.10	5.25	2.08
CS HT Cool.	S HRHT	Q	3.24	0.46	2.33	0.31	0.14	1.53	1.34	0.38
S Boiler	S HRHT	Q	10.87	4.94	5.09	0.75	0.09	6.51	3.82	0.53
S Aux Boiler	S Boiler	Ph	5.71	4.66	0.90	0.17	-0.03	3.77	1.85	0.10
S Aux Boiler	E Env.	Ph	1.51	1.04	0.38	0.08	0.00	0.99	0.50	0.03
S Fuel tank	S Aux Boiler	Ch	20.12	14.37	4.73	1.02	0.01	12.99	6.76	0.37
S HRHT	D HVAC-PH	Q	7.43	1.22	1.89	0.25	0.05	2.29	1.11	0.00
S HRHT	D HVAC-RH	Q	0.33	0.09	0.13	0.03	0.03	0.00	0.00	0.28
S HRHT	D HWH	Q	2.27	0.64	1.09	0.17	0.05	0.84	0.81	0.31
S Boiler	D MSH	Q	0.68	0.06	0.10	0.01	0.00	0.09	0.07	0.02
S Boiler	D HFO TH	Q	0.66	0.13	0.20	0.03	0.01	0.16	0.16	0.04
S Boiler	D HFO H	Q	0.44	0.04	0.21	0.03	0.02	0.13	0.12	0.04
S Boiler	D TH	Q	0.51	0.08	0.12	0.02	0.01	0.11	0.10	0.03
S Boiler	D G	Q	2.45	0.44	0.98	0.14	0.04	0.71	0.69	0.19
S Boiler	D OT	Q	0.34	0.08	0.12	0.02	0.01	0.11	0.10	0.03
EL SB	EL Thrusters	W	0.94	0.00	0.00	0.94	0.00	0.36	0.43	0.15
EL SB	EL HVAC	W	1.79	0.59	0.85	0.18	0.18	0.00	0.00	1.79
EL SB	EL Other el. Dem.	W	59.29	19.99	32.66	4.99	1.64	26.06	25.45	7.78
P Prop. shaft	P Prop.	W	104.19	0.14	82.62	9.84	11.59	40.98	44.55	18.66
P Prop. shaft	E Losses	Q	3.20	0.00	2.54	0.30	0.36	1.26	1.37	0.57
S Boiler	E Dumped steam	Q	0.81	0.00	0.43	0.13	0.25	0.05	0.20	0.55

Table B.14: Summary of exergy flows for the boiler and steam systems

	From	To	Type	Total	P/S	LSS	Man	HSS	Win	Mid	Sum	
D	HVAC-PH	D	Dem.	Q	3.41	1.22	1.89	0.25	0.05	2.29	1.11	0.00
D	HVAC-RH	D	Dem.	Q	0.28	0.09	0.13	0.03	0.03	0.00	0.00	0.28
D	HWH	D	Dem.	Q	1.96	0.64	1.09	0.17	0.05	0.84	0.81	0.31
D	MSH	D	Dem.	Q	0.18	0.06	0.10	0.01	0.00	0.09	0.07	0.02
D	HFO TH	D	Dem.	Q	0.37	0.13	0.20	0.03	0.01	0.16	0.16	0.04
D	HFO H	D	Dem.	Q	0.29	0.04	0.21	0.03	0.02	0.13	0.12	0.04
D	TH	D	Dem.	Q	0.23	0.08	0.12	0.02	0.01	0.11	0.10	0.03
D	G	D	Dem.	Q	1.59	0.44	0.98	0.14	0.04	0.71	0.69	0.19
D	OT	D	Dem.	Q	0.15	0.05	0.08	0.01	0.00	0.07	0.07	0.02

Table B.15: Summary of exergy flows for the heating demand

Appendix C. Full list of available measurements

References

- [1] T.W.P. Smith, J. P. Jalkanen, B.A. Anderson, James J Corbett, J. Faber, Hanayama S., E. O'Keeffe, S. Parker, L. Johansson, L. Aldous, C. Raucci, M. Traut, S. Ettinger, D. S. Lee, S. Ng, A. Agrawal, James J Winebrake, M. Hoen, S. Chesworth, and A. Pandey. Third IMO GHG Study. Technical report, International Maritime Organization (IMO), London, UK, 2014.
- [2] UNCTAD. Review of maritime transport. united conference on trade and development.
- [3] Karin Andersson, Selma Brynolf, J Fredrik Lindgren, and Magda Wilewska-Bien. *Shipping and the Environment*. Springer, Berlin, Germany, 2016.
- [4] Cruise Lines International Association. 2018 Cruise Industry Outlook. Technical report, 2017.
- [5] Eke Eijgelaar, Carla Thaper, and Paul Peeters. Antarctic cruise tourism: the paradoxes of ambassadorship, last chance tourism and greenhouse gas emissions. *Journal of Sustainable Tourism*, 18(3):337–354, April 2010.
- [6] Karla Poplawski, Eleanor Setton, Bryan McEwen, Dan Hrebenyk, Mark Graham, and Peter Keller. Impact of cruise ship emissions in Victoria, BC, Canada. *Atmospheric Environment*, 45(4):824–833, February 2011.
- [7] Nickie Butt. The impact of cruise ship generated waste on home ports and ports of call: A study of Southampton. *Marine Policy*, 31(5):591–598, September 2007.
- [8] Juan Gabriel Brida and Sandra Zapata. Cruise tourism: economic, socio-cultural and environmental impacts. *International Journal of Leisure and Tourism Marketing*, 1(3):205–226, December 2009.
- [9] Evert A Bouman, Elizabeth Lindstad, Agathe I Rialland, and Anders H Strømmann. State-of-the-art technologies, measures, and potential for reducing ghg emissions from shipping—a review. *Transportation Research Part D: Transport and Environment*, 52:408–421, 2017.

- [10] W. Shi, D. Stapersma, and H. T. Grimmelius. Analysis of energy conversion in ship propulsion system in off-design operation conditions. *WIT Transactions on Ecology and the Environment*, 121:449–460, 2009.
- [11] Gerasimos Theotokatos and Vasileios Tzelepis. A computational study on the performance and emission parameters mapping of a ship propulsion system. *Proceedings of the Institution of Mechanical Engineers, Part M : Journal of Engineering for the Maritime Environment*, 229(1):58–76, 2015.
- [12] F. Tillig, J. Ringsberg, W. Mao, and B. Ramne. A generic energy systems model for efficient ship design and operation. *Proceedings of the Institution of Mechanical Engineers, Part M: Journal of Engineering for the Maritime Environment*, 2016.
- [13] G Thomas, D O’Doherty, D Sterling, and C Chin. Energy audit of fishing vessels. *Proceedings of the Institution of Mechanical Engineers, Part M: Journal of Engineering for the Maritime Environment*, 224(November 2009):87–101, 2010.
- [14] Oihane C. Basurko, Gorka Gabi??a, and Zigor Uriondo. Energy performance of fishing vessels and potential savings. *Journal of Cleaner Production*, 54:30–40, 2013.
- [15] Charlotte Banks, Osman Turan, Atilla Incecik, G. Theotokatos, Sila Izkan, Catherine Shewell, and Xiaoshuang Tian. Understanding Ship Operating Profiles with an Aim to Improve Energy Efficient Ship Operations. In *Proceedings of the Low Carbon Shipping Conference*, pages 1–11, 2013.
- [16] a. Coraddu, M. Figari, and S. Savio. Numerical investigation on ship energy efficiency by Monte Carlo simulation. *Proceedings of the Institution of Mechanical Engineers, Part M: Journal of Engineering for the Maritime Environment*, 228(3):220–234, 2014.
- [17] Francesco Baldi, Gerasimos Theotokatos, and Karin Andersson. Development of a combined mean value-zero dimensional model and application for a large marine four-stroke Diesel engine simulation. *Applied Energy*, 154:402–415, 2015.

- [18] Francesco Baldi and Cecilia Gabrielii. A feasibility analysis of waste heat recovery systems for marine applications. *Energy*, 80:654–665, 2015.
- [19] Byung Chul Choi and Young Min Kim. Thermodynamic analysis of a dual loop heat recovery system with trilateral cycle applied to exhaust gases of internal combustion engine for propulsion of the 6800 TEU container ship. *Energy*, 58:404–416, 2013.
- [20] H. Ghassemi and H. Zakerdoost. Ship hull-propeller system optimization based on the multi-objective evolutionary algorithm. *Proceedings of the Institution of Mechanical Engineers, Part C: Journal of Mechanical Engineering Science*, 231(1):175–192, 2017.
- [21] S. Solem, K. Fagerholt, S.O. Erikstad, and . Patricksson. Optimization of diesel electric machinery system configuration in conceptual ship design. *Journal of Marine Science and Technology (Japan)*, 20(3):406–416, 2015.
- [22] F. Baldi, H. Johnson, C. Gabrielii, and K. Andersson. Energy and exergy analysis of ship energy systems - The case study of a chemical tanker. *International Journal of Thermodynamics*, 18(2):82–93, 2015.
- [23] G. Theotokatos and G. Livanos. Techno-economical analysis of single pressure exhaust gas waste heat recovery systems in marine propulsion plants. *Proceedings of the Institution of Mechanical Engineers, Part M: Journal of Engineering for the Maritime Environment*, 227(2):83–97, 2012.
- [24] Dimitrios T Hountalas, Georgios C Mavropoulos, and Christos Katsanos. Efficiency Optimization of a 2-Stroke Diesel Engine Power Plant Through the Recovery of Exhaust Gas Using a Rankine Cycle. *International Conference on Efficiency, Cost, Optimization, Simulation and Environmental Impact of Energy Systems*, pages 1–17, 2012.
- [25] George G. Dimopoulos, Chariklia A. Georgopoulou, and Nikolaos M. P. Kakalis. The introduction of exergy analysis to the thermo-economic modelling and optimisation of a marine combined cycle system. *Proceedings of the 25th International Conference on Efficiency, Cost, Optimization, Simulation and Environmental Impact Of energy Systems*, pages 221–236, 2012.

- [26] Maria E. Mondejar, Fredrik Ahlgren, Marcus Thern, and Magnus Genrup. Quasi-steady state simulation of an organic Rankine cycle for waste heat recovery in a passenger vessel. *Applied Energy*, 185:1324–1335, 2017.
- [27] Anthony F Molland. *The maritime engineering reference book: a guide to ship design, construction and operation*. Elsevier, 2011.
- [28] WL McCarthy, WS Peters, and DR Rodger. Marine diesel power plant practices, 1990.
- [29] R Balaji and Omar Yaakob. An analysis of shipboard waste heat availability for ballast water treatment. *Journal of Marine Engineering & Technology*, 11(2):15–29, 2012.
- [30] Waltteri Salmi, Juha Vanttola, Mia Elg, Maunu Kuosa, and Risto Lahdelma. Using waste heat of ship as energy source for an absorption refrigeration system. *Applied Thermal Engineering*, 115:501–516, 2017.
- [31] Gequn Shu, Youcai Liang, Haiqiao Wei, Hua Tian, Jian Zhao, and Lina Liu. A review of waste heat recovery on two-stroke IC engine aboard ships. *Renewable and Sustainable Energy Reviews*, 19:385–401, 2013.
- [32] Pierre Marty, Philippe Corrigan, Antoine Gondet, Raphaël Chenouard, and JF Hétet. Modelling of energy flows and fuel consumption on board ships: application to a large modern cruise vessel and comparison with sea monitoring data. In *Proceedings of the 11th International Marine Design Conference, Glasgow, UK*, 2012.
- [33] Francesco Baldi, Tuong-Van Nguyen, and Fredrik Ahlgren. The application of process integration to the optimisation of cruise ship energy systems: a case study. In *Proceedings of the 29th International Conference on Efficiency, Cost, Optimization, Simulation and Environmental Impact of Energy Systems*, 2016.
- [34] Pierre Marty, Jean-François Hétet, David Chalet, and Philippe Corrigan. Exergy analysis of complex ship energy systems. *Entropy*, 18(4):127, 2016.

- [35] Turgay Koroglu and Oguz Salim Sogut. Advanced exergy analysis of an organic rankine cycle waste heat recovery system of a marine power plant. *Journal of Thermal Engineering*, 3(2):1136–1148, 2017.
- [36] Adrian Bejan, George Tsatsaronis, Michael Moran, et al. *Thermal design and optimization*. John Wiley & Sons, 1996.
- [37] Tadeusz Jozef Kotas. *The exergy method of thermal plant analysis*. Elsevier, 2013.
- [38] G. Tsatsaronits. Definitions and nomenclature in exergy analysis and exergoeconomics. *Energy*, 32:249–253, 2007.
- [39] Jan Szargut. Chemical exergies of the elements. *Applied Energy*, 32(4):269–286, 1989.
- [40] George Tsatsaronis. Thermo-economic analysis and optimization of energy systems. *Progress in energy and combustion science*, 19(3):227–257, 1993.
- [41] Tapas Kanungo, David M Mount, Nathan S Netanyahu, Christine D Piatko, Ruth Silverman, and Angela Y Wu. An efficient k-means clustering algorithm: Analysis and implementation. *IEEE transactions on pattern analysis and machine intelligence*, 24(7):881–892, 2002.
- [42] Samira Fazlollahi, Stephane Laurent Bungener, Pierre Mandel, Gwenaelle Becker, and Franois Marchal. Multi-objectives, multi-period optimization of district energy systems: I. Selection of typical operating periods. *Computers & Chemical Engineering*, 65:54–66, June 2014.
- [43] Eamonn Keogh, Kaushik Chakrabarti, Michael Pazzani, and Sharad Mehrotra. Locally adaptive dimensionality reduction for indexing large time series databases. *ACM Sigmod Record*, 30(2):151–162, 2001.
- [44] Francesco Baldi, Fredrik Ahlgren, Francesco Melino, Cecilia Gabrielii, and Karin Andersson. Optimal load allocation of complex ship power plants. *Energy Conversion and Management*, 124:344–356, 2016.
- [45] F. Baldi, F. Maréchal, and K. Tammi. Process integration as a tool for the improvement of cruise ships energy efficiency. In *Proceedings of the Shipping in Changing Climate Conference*, London, United Kingdom, sep 2017.

- [46] Fredrik Ahlgren, Maria E. Mondejar, Magnus Genrup, and Marcus Thern. Waste heat recovery in a cruise vessel in the Baltic Sea by using an Organic Rankine Cycle: A case study. *Journal of Engineering for Gas Turbines and Power*, 138(1):011702, 2016.
- [47] Wes McKinney. Data structures for statistical computing in python. In Stéfan van der Walt and Jarrod Millman, editors, *Proceedings of the 9th Python in Science Conference*, pages 51 – 56, 2010.